

CoSMeTIC: Zero-Knowledge Computational Sparse Merkle Trees with Inclusion-Exclusion Proofs for Clinical Research

Mohammad Shahid
 Paritosh Ramanan
 mohshai@okstate.edu
 paritosh.ramanan@okstate.edu
 School of Industrial Engineering and
 Management
 Oklahoma State University
 Stillwater, Oklahoma, USA

Mohammad Fili
 Guiping Hu
 mfilii@gmu.edu
 ghu4@gmu.edu
 George Mason University
 Department of Systems Engineering
 and Operations Research
 Fairfax, Virginia, USA

Hillel Haim
 hillel-haim@uiowa.edu
 University of Iowa
 Department of Microbiology and
 Immunology
 Iowa City, Iowa, USA

Abstract

Analysis of clinical data is a cornerstone of biomedical research with applications in areas such as genomic testing and response characterization of therapeutic drugs. Maintaining strict privacy controls is essential because such data typically contains personally identifiable health information of patients. At the same time, regulatory compliance often requires study managers to demonstrate the integrity and authenticity of participant data used in analyses. Balancing these competing requirements—privacy preservation and verifiable accountability—remains a critical challenge. In this paper, we present CoSMeTIC, a zero-knowledge computational framework that proposes computational Sparse Merkle Trees (SMTs) as a means to generate verifiable inclusion and exclusion proofs for individual participants' data in clinical studies. We formally analyze the zero-knowledge properties of CoSMeTIC and evaluate its computational efficiency through extensive experiments. Using the Kolmogorov–Smirnov and likelihood-ratio hypothesis tests, along with logistic-regression-based genomic analyses on real-world Huntington's disease datasets, we demonstrate that CoSMeTIC achieves strong privacy guarantees while maintaining statistical fidelity. Our results suggest that CoSMeTIC provides a scalable and practical alternative for achieving regulatory compliance with rigorous privacy protection in large-scale clinical research.

Keywords

Zero Knowledge Proof, Sparse Merkle Trees, Regulatory Compliance, Clinical Research Studies.

1 Introduction

Clinical research studies rely on a wide variety of statistical tools and techniques to analyze patient outcomes so as to address the underlying biomedical research questions. Critically, these research questions can potentially help in deciphering the propensity of people to develop certain diseases [33, 50]; formulate statistically robust strategies for their disease prevention [2, 22]; as well as characterize or benchmark responses to therapeutic drugs on a wide demographic base [15, 47]. From a computational perspective however, the underlying techniques could potentially involve using statistical tests to help guide the core clinical research hypothesis [36, 39]; or utilize comparative benchmarking of different statistical models on varying demographic subgroups [46]. Therefore, computational correctness and data accountability are the two

fundamental aspects that govern the integrity of the underlying statistical technique in clinical research studies [3, 17]. Transparently asserting computational correctness and data accountability involves patient privacy risks [5, 25], significant audit burdens on regulating authorities [8] as well as an inability to reliably claim patient exclusion [9, 21]. In this paper, we develop CoSMeTIC, a novel framework to assert computational correctness and user data privacy and accountability in clinical research studies using zero knowledge driven computational sparse Merkle trees (CSMTs).

The CoSMeTIC framework is primarily designed to resolve the three important critical gaps that exist in state of the art clinical research studies. First, ensuring the computational correctness of the study outcome becomes an essential precursor to guarantee the integrity of the clinical study. We define correctness in terms of the order as well as the precision of each computational step that belies the underlying statistical method. Asserting computational correctness in a transparent fashion can potentially help reduce the audit burden on regulatory bodies (such as the U.S. FDA), especially in large scale clinical studies that are geographically spread out. Second, the clinical study must also guarantee data accountability by demonstrating that the study outcomes are based on genuine patient data records. As part of the data accountability argument, the clinical study manager must also be capable of providing individual patients an inclusion or exclusion receipt pertaining to the use of their respective data records. Lastly, the entire computational graph from the raw user data to the final statistical outcome must be publicly verifiable in a transparent fashion, without the need to divulge identities of the patients or the users.

The CoSMeTIC framework is specifically designed to address problems of computational correctness, patient data privacy and accountability as well as transparency for regulatory authorities. For ensuring correctness, we first decompose the statistical technique into individual computational steps. Consequently, the CoSMeTIC framework leverages computational reductions (CR) which are regarded as the basic building blocks for statistics and data analytics [6, 7]. CR primitives have been widely used for carrying out large-scale data science and analytics pipelines and are the core drivers behind large scale compute frameworks such as Apache Spark [48] as well as Message Passing Interface (MPI) [7]. As a result, a series of CR primitives can be used to formally map each computational step involved in a statistical technique recursively from raw user data to the final statistical output. In this paper, we leverage CSMTs

to represent each CR operation involved in the statistical method to enable membership proofs for distinct computational steps.

Conventionally, plain sparse Merkle Trees (SMTs) are defined on the basis of leaf space cardinality which must be equivalent to the output bit space of the hashing algorithm employed to construct the tree. By notionally equating the set of potential leaves with the set of total possible outcomes of a hash algorithm, an SMT can deliver inclusion as well as exclusion proofs for individual data records [19, 43]. However, the conventional SMT architecture relies on simple hash concatenation applied at each level of the tree which is fundamentally incompatible with the CR operations that seek to aggregate data across the entire clinical user dataset. As a result, it becomes significantly challenging to provide a verifiable computational trace regarding the statistical methodology of clinical studies while retaining user privacy and clinical audit efficiency.

In order to alleviate the CR-oriented limitations of the Merkle tree architecture, we propose the CSMT architecture that promises the potential of delivering user membership proofs with respect to individual computational steps themselves. In CoSMeTIC each CSMT represents one CR step with the corresponding primitive applied at each level of the Merkle tree. As a result, the CoSMeTIC framework enables user inclusion and exclusion proofs at each CR step of the statistical technique used in the clinical study. To induce transparency, we augment the CSMT architecture with publicly verifiable, zero-knowledge proofs that can assert the integrity of the data transformation and aggregation with complete privacy of the individual user. These zero-knowledge proofs rely on the zk-SNARK (Succinct, Non-interactive, Argument of Knowledge) paradigm and help assert the overall integrity of the entire statistical technique, capturing every transformation of raw user data records among a series of zk-SNARKs.

The CoSMeTIC framework delivers key benefits for both regulators and patients by addressing three critical gaps relating to computational correctness, data accountability, and privacy-preserving transparency. For regulators, CoSMeTIC enables efficient public verification of the correct execution of statistical methods underlying clinical study claims, significantly reducing audit burdens and potentially accelerating regulatory clearance. For patients and data contributors, the framework provides strong data governance guarantees through verifiable inclusion receipts and exclusion proofs, ensuring consent and accountability. Finally, publicly verifiable zk-SNARK proofs for leaf transformations and Merkle tree traversal offer transparent, end-to-end visibility into the study's computational pipeline, allowing patients to understand precisely how their data was used and enabling regulators to pinpoint the exact role of individual records within the overall analysis.

Our work showcases the efficacy of the CoSMeTIC framework with respect to different statistical methods as well as real world case studies. Primarily we leverage datasets pertaining to Huntington's disease as well as the Temsavir antiviral therapeutic drug for human immunodeficiency virus type 1 (HIV-1) as the experimental foundation for our work. Using these datasets we formulate clinical research studies involving the Kolmogorov Smirnov (KS) statistical hypothesis tests as well as accuracy and Likelihood Ratio tests (LRT) to benchmark the relative performance of logistic regression models. Our contributions can be summarized as follows:

- We develop a Computational Sparse Merkle Tree (CSMT) module that integrates CR primitives with the Merkle tree architecture that is capable of providing inclusion and exclusion proofs for individual computational steps as a means for privacy and accountability.
- We build a zk-SNARK driven framework that encodes the entire graph of CR primitives in zero-knowledge providing end-to-end transparency of the clinical study.
- We provide theoretical security guarantees regarding the robustness of the zero-knowledge framework that delivers patient data privacy, accountability and transparency.
- We demonstrate the performance of the framework on a wide range of statistical methods involving the KS hypothesis test as well as the LRT and accuracy tests for logistic regression applied towards the clinical datasets.

We now proceed to summarize the related work pertaining to SMTs in addition to a brief review of current state of the art methods in the domain of verifiable statistics.

2 Related Work

In recent years, there are strong emerging research trends pertaining to verifiable statistics. Custodes [38] certifies classical hypothesis tests (e.g., t -tests, χ^2 tests, ANOVA) by logging encrypted test evaluations and issuing cryptographically certified p -values, thereby deterring p -hacking. Verifiable differential privacy (VerDP) [30] and its follow-ups use zero-knowledge proofs to show that randomized mechanisms (e.g., Laplace noise for counts) have been applied correctly to sensitive data before releasing aggregate statistics. RiseFL [51] embeds a χ^2 -style goodness-of-fit test into a low-cost SNARK circuit to verify that federated-learning updates satisfy certain norm bounds, and ElectionGuard-based protocols [23] combine per-ballot zero-knowledge proofs with risk-limiting audits to statistically validate election outcomes.

While all of these works focus on verifiable statistics, they lack the ability to account for datum-level accountability. These systems demonstrate that hypothesis tests and related statistical procedures can be implemented inside zero-knowledge circuits, but they treat the underlying dataset as a monolithic object. The cryptographic guarantees apply to the correctness of the *global* test statistic or mechanism, not to verifiable claims about whether any specific individual's datum was included or excluded from the analysis.

Existing work that targets privacy-preserving user-level data accountability, has made significant progress but only in terms of user-data oriented state accountability. Transparency dictionaries such as Verdict [43] introduce indexed Merkle trees that support succinct inclusion and non-inclusion proofs over a 2^{256} -sized key space and can be combined with SNARK backends for lazy, on-demand verification. IMOK [19] extends sparse Merkle trees (SMTs) with non-prohibition proofs for sanction lists, while Cartesian Merkle Trees (CMTs) [4] and related constructions optimize membership and non-membership proofs for blockchain and rollup settings. Recent compliance-oriented systems, such as private smart wallets with probabilistic compliance [35], likewise use SMTs to certify that a given account is (or is not) contained in a prohibited set.

However, in all of these designs, Merkle leaves are treated as *static key-value records*, and the associated zero-knowledge circuits implement only lookup, append-only, or simple boolean predicates. None of these systems implements a *computational SMT* or Merkle-sum SMT that is capable of supporting arbitrary per-leaf transformations and numeric reductions over selected leaves. Further, they lack the capability of providing inclusion and exclusion proofs with respect to the aggregated reductions over individual datum belonging to specific users. Proof-of-solvency protocols based on Merkle-sum trees [13] do realize aggregation semantics at internal nodes, but typically over dense trees, without published non-membership circuits, and in financial rather than statistical-testing settings. Therefore, there exists a critical gap that needs to be bridged between the *state accountability* of the data, and the *analysis accountability* at the granularity of individual datum that is required in clinical studies. Additionally, for implementing these missing capabilities, we need novel methodologies that scale to sparse 2^{256} key spaces while keeping proof generation lazy and participant-driven.

Taken together, the two strands of verifiable statistic and analysis accountability leave a critical gap for privacy-sensitive scientific domains such as clinical studies. On one side, SMT-based ZK frameworks provide efficient inclusion and non-inclusion proofs but are largely agnostic to the statistical computations performed over the committed dataset, and they lack Merkle-sum semantics tailored to complex tests. On the other side, ZK-based verifiable statistics frameworks ensure that certain hypothesis tests are executed correctly, but they do not cryptographically bind the test inputs to a fine-grained, participant-auditable commitment structure. In particular, they do not offer a way for a participant to ask, *ex post*, “Was my data used in this KS test, likelihood-ratio test, or regression model?” and receive a provable inclusion or non-inclusion proof tied to that exact computation. As a result, there is a clear lack of supporting methodologies that can provide individual-level data accountability with provable membership guarantees in aggregations over pre-defined user datasets.

To the best of our knowledge, there is no existing framework that (i) instantiates a *computational* sparse Merkle tree in which internal nodes encode analysis-specific reductions (e.g., transformed sufficient statistics for KS or likelihood-ratio tests), (ii) supports both inclusion and exclusion proofs for individual participants with respect to a given statistical pipeline, (iii) provides a scalable extensible framework for applications with a large number of aggregation operations, and (iv) demonstrates these guarantees on real-world clinical datasets without degrading the fidelity of downstream hypothesis tests. CoSMeTIC is designed to precisely fill this gap by combining SMT-based, participant-centric accountability with zero-knowledge implementations of classical hypothesis tests and regression models used in large-scale clinical research.

3 Problem Formulation

We consider a group of n users denoted by $U = \{u_1, u_2, \dots, u_n\}$ wherein each user u_i possesses the raw datum $\delta_i \in \mathbb{R}^d$ leading to a user group dataset denoted by Δ_U as denoted in Equation (1).

$$\Delta_U = [\delta_1 \dots \delta_n] \quad (1)$$

Further, we consider a computational scheme consisting of a leaf transformation function denoted by \mathcal{L} and an aggregator function denoted by \mathcal{A} parametrized by $\theta_{\mathcal{L}}, \theta_{\mathcal{A}}$ respectively as defined in Equations (2), (3). Their composite can be denoted as $\mathcal{A} \circ \mathcal{L}$ as defined in Equation (4) respectively.

$$\mathcal{L} : \mathbb{R}^d \mapsto \mathbb{R}^p \quad (2)$$

$$\mathcal{A} : \mathbb{R}^{p \times n} \mapsto \mathbb{R}^p \quad (3)$$

$$\mathcal{A} \circ \mathcal{L} : \mathbb{R}^{d \times n} \mapsto \mathbb{R}^p \quad (4)$$

The leaf transformation \mathcal{L} is geared towards transformation of raw datum of individual users leading to a user group specific transformed dataset $\Delta_U^{\mathcal{L}}$ as denoted in Equation (5). On the other hand, the application of the aggregation \mathcal{A} on set $\Delta_U^{\mathcal{L}}$ results in a reduction denoted by $R(\mathcal{A}, \mathcal{L}, U)$ as given in Equation (6).

$$\Delta_U^{\mathcal{L}} = [\mathcal{L}(\delta_1; \theta_{\mathcal{L}}), \mathcal{L}(\delta_2; \theta_{\mathcal{L}}), \dots, \mathcal{L}(\delta_n; \theta_{\mathcal{L}})] \quad (5)$$

$$R(\mathcal{A}, \mathcal{L}, U) = \mathcal{A}(\Delta_U^{\mathcal{L}}; \theta_{\mathcal{A}}) \quad (6)$$

The reduction $R(\mathcal{A}, \mathcal{L}, U)$ represents the aggregated outcome (e.g., statistical summary, model update, etc.) computed from the transformed dataset.

In order to formalize the objective of clinical stakeholders, we first define computational membership using function \mathcal{M} as presented in Definition 1.

DEFINITION 1 (COMPUTATIONAL MEMBERSHIP). *Given an arbitrary user identity \tilde{u} with raw datum $\tilde{\delta}$, the membership function can be defined by \mathcal{M}*

$$\mathcal{M}([\tilde{u}, \tilde{\delta}] | R) = \begin{cases} 1, & \text{if } \mathcal{L}(\tilde{\delta}) \in \Delta_U^{\mathcal{L}} \text{ and } R = \mathcal{A}(\Delta_U^{\mathcal{L}}) \\ 0, & \text{otherwise} \end{cases}$$

where U, Δ_U denote a pre-defined user identity set and its corresponding user group dataset for a given leaf transform \mathcal{L} and an aggregation function \mathcal{A}

With the help of Definition 1, we formally state the prover objective using Definition 2 for an arbitrary user identity \tilde{u} with a datum corresponding to $\tilde{\delta}$.

DEFINITION 2 (CLINICAL STAKEHOLDER OBJECTIVE). *Given a user identity set U , its corresponding user group dataset Δ_U and the resulting global reduction $R(\mathcal{A}, \mathcal{L}, U)$ the clinical stakeholder objective is to provide a publicly verifiable proof of membership or non-membership of an arbitrary user identity \tilde{u} by evaluating the membership function $\mathcal{M}([\tilde{u}, \tilde{\delta}] | R(\mathcal{A}, \mathcal{L}, U))$ without disclosing Δ_U or any other intermediate transformations.*

Definition 2 provides a fundamental overview of the task of the clinical stakeholder which is responsible of handling patient datasets. Regulatory mandates would encumber the clinical stakeholder to demonstrate the use of data pertaining to specific individuals. For the regulator, this would help enforce compliance requirements regarding the integrity of the underlying datasets used in clinical trials.

3.1 User Identity Management

For implementing the SMT, we must first ensure that raw user datum is uniquely coupled with their corresponding identity. Additionally, depending on the nature of \mathcal{L} , there is a non-trivial probability of the user salted data of two users mapping to the same transformed output. Therefore, we must also ensure that transformed outputs are uniquely distinguishable across different users.

Asserting User Identity: We rely on user salts to uniquely assert the identity of the user as well as to enable them to demonstrate ownership of their datum as elaborated in Property 1.

PROPERTY 1. *The identity of a user $u_i \in U$ can be uniquely bound to their corresponding datum δ_i through a secret salt vector $\mu_i \in \mathbb{R}^{s_u}$.*

Specifically, for each user identity u , the corresponding datum is concatenated with a user salt $\mu \in \mathbb{R}^{s_u}$ leading to $\delta^s \equiv (\delta, \mu)$. The user salt μ is a secret vector of s_u dimension uniquely held only by the user and must not be revealed or made public. As a consequence we obtain a salted user group dataset denoted by Δ_U^s in Equation (7).

$$\Delta_U^s = \left[(\delta_1, \mu_1), (\delta_2, \mu_2) \dots (\delta_n, \mu_n) \right] \quad (7)$$

$$\hat{\mathcal{L}} : \mathbb{R}^{d+s_u} \mapsto \mathbb{R}^p \quad (8)$$

The unique salt binding for each user ensures that each record in Δ_U^s is uniquely attributable to its originating user. In order to handle the transformations of the salted user datum, we modify the leaf transform input dimension to yield $\hat{\mathcal{L}}$ parametrized by $\theta_{\hat{\mathcal{L}}}$ as denoted in Equation (8).

Asserting Uniqueness of Leaf Transformation: For enforcing distinguishability between transformed outputs of different users, we concatenate a user specific transform salt to the leaf transform output of salted user datum as described by Property 4.

PROPERTY 2. *The leaf transformation of the salted user datum (δ_i, μ_i) of user $u_i \in U$ can be made uniquely distinguishable across user set U by binding the outputs of the modified leaf transform function $\hat{\mathcal{L}}(\delta_i, \mu_i)$ with a secret transform salt vector $\tau_i \in \mathbb{R}^{s_t}$.*

Specifically, for a given user u with raw datum and user salt represented by δ, μ respectively, we incorporate $\tau \in \mathbb{R}^{s_t}$ such that Equation (9) holds.

$$\mathcal{L}^s([\delta, \mu, \tau]; \theta_{\mathcal{L}^s}) = [\hat{\mathcal{L}}(\delta, \mu; \theta_{\hat{\mathcal{L}}}), \tau], \quad \tau \in \mathbb{R}^{s_t} \quad (9)$$

Consequently, we obtain a user group specific salted leaf transform dataset pertaining to set of users U as denoted by $\Delta_U^{\mathcal{L}^s}$ in Equation (10).

$$\Delta_U^{\mathcal{L}^s} = [\mathcal{L}^s([\delta_1, \mu_1, \tau_1]; \theta_{\mathcal{L}^s}), \dots, \mathcal{L}^s([\delta_n, \mu_n, \tau_n]; \theta_{\mathcal{L}^s})] \quad (10)$$

As a result of using the transform salt, the output dimension of the leaf transform will also change effectively changing the dimensions of the aggregator as well. Therefore, the modified leaf transform and aggregator function can be denoted would acquire the mappings represented in Equations (11)-(13).

$$\mathcal{L}^s : \mathbb{R}^{d+s_u} \mapsto \mathbb{R}^{p+s_t} \quad (11)$$

$$\mathcal{A}^s : \mathbb{R}^{(p+s_u) \times n} \mapsto \mathbb{R}^{p+s_t} \quad (12)$$

$$\mathcal{A}^s \circ \mathcal{L}^s : \mathbb{R}^{(d+s_u) \times n} \mapsto \mathbb{R}^{p+s_t} \quad (13)$$

3.2 Computational Sparse Merkle Trees

We consider Sparse Merkle Trees (SMT) as a means to represent the computational graph pertaining to the global aggregation function \mathcal{A}^s parametrized by $\theta_{\mathcal{A}^s}$. SMTs are a sparse version of conventional Merkle trees which rely on a well-formed hash function that provides one-wayness, hiding and collision resistance properties [28]. We formally define a hash function in Definition 3.

DEFINITION 3 (HASH FUNCTION). *A hash function denoted by hash can be defined such that it can consume arbitrary length inputs so as to map to fixed length outputs of size K*

$$\text{hash} : \{0, 1\}^* \rightarrow \{0, 1\}^K$$

Sparse Merkle Trees (SMTs) differ from conventional Merkle trees in both tree height and the number of leaf nodes. For a hash function producing an output of K bits, a traditional Merkle tree has a variable height that depends on the number of data elements included as leaves. In contrast, an SMT consists of 2^K leaves resulting in a fixed tree height of K . Given a set of data elements, the construction of an SMT relies on determining the hash string of each element. The binary representation of each hash string determines the leaf position of the corresponding data element while the unfilled leaf positions are characterized by the hash of a default element. Starting from the leaves, the conventional version of the SMT is constructed by recursively hashing the concatenation of hash strings of two adjacent elements ultimately culminating in the root element.

Unlike conventional Sparse Merkle Trees (SMTs), which recursively concatenate and hash child nodes, the *computational* variant performs a reduction operation at each recursion level. Specifically, we view the global aggregation function \mathcal{A}^s as a recursive composition of local reduction functions $\mathcal{A}^l(\cdot; \theta_{\mathcal{A}^l})$, where each \mathcal{A}^l combines the aggregated values of two child nodes into a higher-level representation as denoted in Equation (14).

$$\begin{aligned} \mathcal{A}^s(\Delta_U^{\mathcal{L}^s}; \theta_{\mathcal{A}^s}) = \\ \mathcal{A}_{(K)}^l(\mathcal{A}_{(K-1)}^l(\dots \mathcal{A}_{(0)}^l(\varphi_L^L, \varphi_R^L; \theta_{\mathcal{A}_l}) \dots; \theta_{\mathcal{A}_l}); \theta_{\mathcal{A}_l}) \end{aligned} \quad (14)$$

This recursive construction yields a *Computational Sparse Merkle Tree (CSMT)*, formally defined in Definition 4, for a given user identity set U and their corresponding salted leaf transform set $\Delta_U^{\mathcal{L}^s}$. The relations contained in Definition 4 is illustrated in Figure 1 using three leaf nodes.

DEFINITION 4 (COMPUTATIONAL SPARSE MERKLE TREE (CSMT)). *Given an aggregation function \mathcal{A}^l parametrized by θ , a CSMT is defined as an augmented Sparse Merkle Tree with the following properties.*

$$\begin{aligned} H_i &= \text{hash}(\mathcal{L}^s(\delta_i, \mu_i, \tau_i)) \quad \forall u_i \in U \\ \varphi_j^0 &= \begin{cases} \mathcal{L}^s(\delta_i, \mu_i, \tau_i), & \text{if } \exists u_i \in U \text{ and } H_i = \text{Bin}(j) \\ \mathcal{L}^s(\emptyset), & \text{otherwise} \end{cases} \\ \varphi_P^k &= \mathcal{A}^l(\varphi_L^k, \varphi_R^k; \theta) \quad \forall k \in \{0, \dots, 2^K - 2\} \\ H_P^k &= \text{hash}(\varphi_P^k) \quad \forall k \in \{0, \dots, 2^K - 2\} \\ \varphi^{root} &= R(\mathcal{A}, \mathcal{L}, U) = \mathcal{A}^s(\Delta_U^{\mathcal{L}^s}) \\ H^{root} &= \text{hash}(\mathcal{A}^s(\Delta_U^{\mathcal{L}^s})) \end{aligned}$$

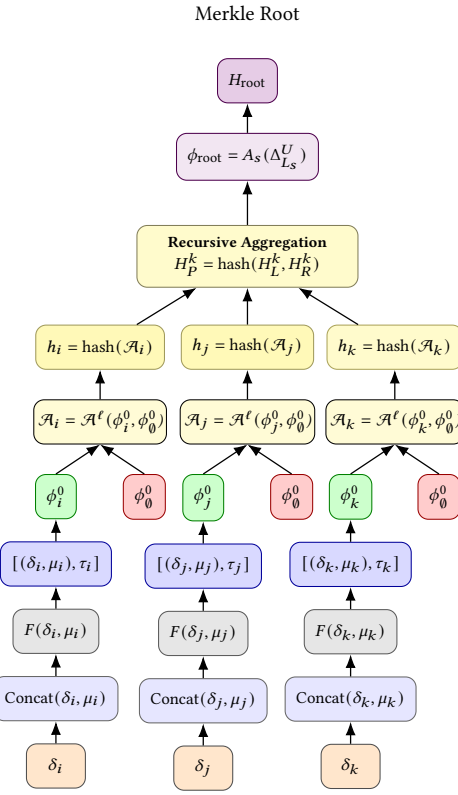


Figure 1: CSMT leaf-level aggregation and hashing.

In Definition 4, φ_j^k and H_j^k denote, respectively, the aggregated value and the corresponding hash at parent node j on level k of the tree. The leaf values φ_j^0 are derived through the salted transformation \mathcal{L}^s over user data $(\delta_i, \mu_i, \tau_i)$, where $\text{Bin}(j)$ represents the binary encoding of the leaf position. Empty leaves are assigned the default salted value $\mathcal{L}^s(\emptyset)$. The root hash H^{root} serves as a global cryptographic commitment to the aggregation outcome φ^{root} which is nothing but the global reduction $\mathcal{A}^s(\Delta_U^Ls) = R(\mathcal{A}, \mathcal{L}, U)$ for all users. Based on the definition of CSMT, we can define the Merkle consistency as defined in Property 3.

PROPERTY 3 (MERKLE CONSISTENCY). *A CSMT is deemed to be consistent if the following conditions apply*

$$H_L^k = H_{L,P}^{k-1} \text{ and } H_R^k = H_{R,P}^{k-1}$$

where $H_{L,P}^{k-1}, H_{R,P}^{k-1}$ denote the hash of the left and right subtree roots and H_L^k and H_R^k denote the children node hashes at tree height k .

As a direct consequence of Definition 4, each leaf in the CSMT admits a unique structural index determined by its salted hash value, formalized in Property 6.

PROPERTY 4 (CSMT INCLUSION). *Given a data tuple (δ, μ, τ) for user $u \in U$, its corresponding leaf node index in the CSMT denoted by \mathcal{N}_u can be computed using the salted leaf transform \mathcal{L}^s as follows.*

$$\mathcal{N}_u = \text{Decimal}[\text{hash}(\mathcal{L}^s(\delta, \mu, \tau))].$$

In other words, Property 4 ensures that each user can be assigned to a unique leaf index \mathcal{N}_u based on the decimal representation of the hash corresponding to their salted leaf transform.

PROPERTY 5 (CSMT EXCLUSION). *Given a leaf node hash H such that*

$$\text{Decimal}(H) = \mathcal{N} \text{ and } \varphi_{\mathcal{N}}^0 = \mathcal{L}^s(\emptyset)$$

then there exists no user $u \in U$ with data tuple corresponding to (δ, μ, τ) that leads to $\text{hash}(\mathcal{L}^s(\delta, \mu, \tau)) = H$, for any combination of $\delta \in \mathbb{R}^d, \mu \in \mathbb{R}^{su}, \tau \in \mathbb{R}^{st}$.

In simpler terms, Property 5 states that a leaf index that maps to the default salted element represents an unoccupied position in the tree.

PROPERTY 6 (CSMT PATH DERIVATION). *Given a leaf node index \mathcal{N} , with the corresponding binary string $\text{Bin}(\mathcal{N}) = [b_1, b_2, \dots, b_K] \in \{0, 1\}^K$ of size K , the path from the CSMT root (denoted by level K) to the \mathcal{N}^{th} leaf node index can be provided based on the following conditions $\forall k \in \{K, K-1, \dots, 1\}$:*

$$b_{K-l+1} = \begin{cases} 0, & \text{move to the left child node,} \\ 1, & \text{move to the right child node.} \end{cases}$$

Property 6 exploits the binary representation of \mathcal{N}_u to derive a path from the root to the leaf node index. More precisely, the path derivation scheme adopts a convention wherein the successive child nodes are determined recursively by examining the current bit value. Moreover, combining Properties 4, 5 and in addition to the one-wayness and collision resistance properties of hash, we can also state that valid Merkle paths are also consistent according to Property 3. Without loss of generality, we denote bit values 0, 1 to represent left and right child nodes respectively.

PROPOSITION 1. *Given a user $u \in U$ with a data tuple (δ, μ, τ) , the CSMT inclusion and exclusion properties form necessary and sufficient conditions for demonstrating membership and non-membership of user u with respect to membership function $\mathcal{M}([u, \delta] \mid R)$, where $R = \mathcal{A}(\Delta_U^L; \theta_{\mathcal{A}})$ denotes the global aggregated reduction across all users while \mathcal{A}, \mathcal{L} represents the unsalted aggregation and leaf transform functions respectively.*

PROOF. Proof provided in Appendix C.1 □

Proposition 1 formally shows that a CSMT can effectively help prove whether a particular user's data record was included in a specific computational aggregation step of the larger statistical method driving the clinical study. In other words, Proposition 1 can help pinpoint the exact computational step where a user's data record has been used to drive the statistical method that underpins the overarching clinical research. Therefore, Proposition 1 has a foundational implication for the CoSMETIC framework since it paves the way for a publicly verifiable zero-knowledge driven mechanism for reliably establishing computational membership claim.

3.3 Zero Knowledge Assertions for CSMTs

We present the preliminaries pertaining to the zero knowledge encapsulations of the Computational Sparse Merkle Tree formulations. More specifically, we consider a zkSNARK framework and

summarize the foundational steps of setup, prove and verify functions imminent in zkSNARKs. Our treatment for CSMTs includes both layers of CSMT pertaining to salted leaf transforms \mathcal{L}^s as well as layered salted aggregation function \mathcal{A}^l .

DEFINITION 5 (zk-SNARK SETUP PHASE). *Given a standard security parameter λ , the zk-SNARK setup phase is defined by the function Setup for both the salted leaf transformation and aggregation functions as follows:*

$$\begin{aligned} \text{Setup}(1^\lambda, \mathcal{L}^s, \theta_{\mathcal{L}^s}) &\mapsto (pk_{\mathcal{L}^s}, vk_{\mathcal{L}^s}), \\ \text{Setup}(1^\lambda, \mathcal{A}^l, \theta_{\mathcal{A}^l}) &\mapsto (pk_{\mathcal{A}^l}, vk_{\mathcal{A}^l}). \end{aligned}$$

The setup phase in Definition 5 generates the proving and verification key pairs (pk, vk) corresponding to the functions \mathcal{L}^s and \mathcal{A}^l . This phase is typically executed once per circuit instantiation and is parameterized by the model weights θ . Since the underlying state-space model \mathcal{M} is pretrained and stable, the setup need not be repeated frequently. However, any modification to θ —such as retraining or parameter updates—necessitates re-execution of the setup phase.

DEFINITION 6 (zk-SNARK PROVING PHASE). *The zk-SNARK proof generation phase is defined by the function Prove as follows:*

$$\begin{aligned} \text{Prove}(pk_{\mathcal{L}^s}, \theta_{\mathcal{L}^s}, \mathcal{L}^s, [\delta, \mu], \mathcal{L}^s(\delta, \mu, \tau)) &\mapsto \Pi_{\mathcal{L}^s}^u, \\ \text{Prove}(pk_{\mathcal{A}^l}, \theta_{\mathcal{A}^l}, \mathcal{A}^l, [\varphi_L^k, \varphi_R^k], \mathcal{A}^l(\varphi_L^k, \varphi_R^k)) &\mapsto \Pi_{\mathcal{A}^l}^k. \end{aligned}$$

Definition 6 specifies the proof generation step. The Prove function takes as input the proving key pk , the function parameters θ , and the corresponding witness–statement pairs $([\delta, \mu], \mathcal{L}^s(\delta, \mu, \tau))$ for the leaf transformation, or $([\varphi_L^k, \varphi_R^k], \mathcal{A}^l(\varphi_L^k, \varphi_R^k))$ for the aggregation step. It outputs a proof artifact Π , which attests to the correct evaluation of the underlying function in zero knowledge. Proofs are generated independently at each layer or recursion depth of the CSMT.

DEFINITION 7 (zk-SNARK VERIFICATION PHASE). *The verification phase of the zk-SNARK protocol is defined by the function Verify as follows:*

$$\text{Verify}(vk_{\mathcal{L}^s}, \Pi_{\mathcal{L}^s}^u) \mapsto \Phi_{\mathcal{L}^s}^u, \text{ and } \text{Verify}(vk_{\mathcal{A}^l}, \Pi_{\mathcal{A}^l}^k) \mapsto \Phi_{\mathcal{A}^l}^{u,k}.$$

Definition 7 describes the verification step, in which a verifier uses the verification key vk to validate a proof Π corresponding to a given function execution. The Verify function outputs a Boolean flag $\Phi \in \{0, 1\}$ indicating whether the proof is valid. In practice, this allows regulators or auditors to confirm that each reported computation—whether at the leaf or aggregation level—was performed correctly, without requiring access to the underlying private data. For notational simplicity, we refer to leaf transform and Merkle path proofs by the acronyms LTR and MRP proofs respectively. As a consequence of Definition 6, we collate the set of LTR and MRP proof artifacts into a distinct proof tuple denoted by Π_{CSMT}^u for every user as denoted by Equation (15).

$$\text{LTR Proof : } \Pi_{\mathcal{L}^s}^u, \text{ MRP Proof Set : } \Pi_{\mathcal{A}^l}^{u,1:K} = \{\Pi_{\mathcal{A}^l}^{u,1}, \dots, \Pi_{\mathcal{A}^l}^{u,K}\} \quad (15)$$

$$\text{CSMT Proof Set : } \Pi_{\text{CSMT}}^u = \left[\Pi_{\mathcal{L}^s}^u, \Pi_{\mathcal{A}^l}^{u,1:K} \right] \quad (16)$$

PROPOSITION 2. *Given a user u and individual datum δ , an aggregated reduction value $\mathcal{R}(\mathcal{A}, \mathcal{L}, U)$ and the proof tuple set Π_{CSMT}^u , and consistent $vk_{\mathcal{L}^s}, vk_{\mathcal{A}^l}$, the following conditions are necessary and sufficient for realizing the membership function $\mathcal{M}([u, \delta] | \mathcal{R}(\mathcal{A}, \mathcal{L}, U))$*

$$\Phi_{\mathcal{L}^s}^u = 1 \text{ and } \Phi_{\mathcal{A}^l}^{u,k} = 1, \quad \forall k \in \{1, K\}$$

PROOF. Proof given in Appendix C.2 \square

Proposition 2 shows that the successful public verification of each individual zk-SNARK artifacts in the set Π_{CSMT}^u can help demonstrate the utilization (or lack thereof), of a user data record to drive an individual aggregation step that is implemented through a CSMT. At a fundamental level, Proposition 2 helps realize the implications of Proposition 1 purely in terms of zk-SNARKs. Proposition 2 ensures that the set of zk-SNARKs contained in Π_{CSMT}^u serve as the inclusion or exclusion guarantees for user datasets.

4 Algorithmic Foundations of CoSMETIC

We construct the algorithmic foundation of the CoSMETIC framework by discussing the set of infrastructure assumptions, followed by the algorithmic components pertaining to the prover and verifier.

4.1 Assumptions

The assumptions for the CoSMETIC framework encompass both endogenous as well as exogenous factors pertaining to data storage and trusted setups that are vital for the success of the zk-SNARK driven architecture.

ASSUMPTION 1 (PHR DATABASE). *The raw data record and user salt δ_u, μ_u along with a unique transform salt τ_u of each user u are part of a personal health record (PHR) database capable of providing publicly verifiable membership proofs of individual user datum.*

Assumption 1 postulates the existence of a personal health record (PHR) database that stores and manages raw data record, user and transform salt. Additionally, we also assume that the PHR database is capable of providing Merkle membership proofs of $(\text{hash}(\delta_u, \mu_u), \text{hash}(\tau_u))$ through simple Merkle trees. The primary advantage of doing so would be to prevent data tampering or misuse of user data records in the clinical study itself. CoSMETIC also supports multiple such PHR databases that store data for different users participating in a single study, provided that each database can substantiate user records through simple Merkle proofs.

ASSUMPTION 2 (TRUSTED ENVIRONMENT). *A trustworthy, secure environment exists which:*

- (1) *guarantees the existence of a Common Reference String (CRS) for zk-SNARK generation, through a publicly verifiable ceremony.*
- (2) *generates proving and verification keys, as part of the zk-SNARK setup phase.*

Assumption 2 discusses the presence of a trustworthy environment where the proving and verification keys for zk-SNARK circuits are generated as part of the setup phase. The implementation of the CoSMETIC is based on the ezk1 framework [41] which uses the Halo2 proof generation backend. As a result, our proof generation depends on elliptic-curve cryptographic primitives and on the integrity of the Common Reference String (CRS) which we assume is generated through a publicly verifiable ceremony.

ASSUMPTION 3 (CLINICAL RESEARCH ORGANIZATION (CRO)). A CRO exists that governs the implementation of the study by:

- (1) acquiring user data from the PHR database.
- (2) delivering CSMT zk-SNARK artifacts with LTR and MRP proofs.
- (3) publicly disclosing MRP and LTR proofs for each user.

Assumption 3 assumes the existence of a clinical research organization (CRO) which is the driver of the entire clinical research study. The CRO is assumed to handle the acquisition of user data and corresponding transform salts of each user from the PHR database; as well as generating and disclosing proof artifacts. It is not necessary for the the CRO and the trusted environment assumed in Assumption 2 to be identical. In fact, the CoSMETIC architecture allows these two entities to be distinct in the real-world. As a result, scenarios wherein a third party, such as a regulatory authority, generates and delivers the zk-SNARK circuits for the CRO to carry out the clinical study is plausible.

Based on Assumptions 1, 2 and 3, we now discuss the algorithm design of the CoSMETIC architecture.

4.2 CRO Oriented Algorithmic Components

The CRO side algorithmic components broadly handles tasks pertaining to leaf transformations, CSMT construction and generation of corresponding zk-SNARKS. For brevity, we abstract away operations pertaining to private data storage on the CRO side.

4.2.1 Salted Leaf Transforms : In Algorithm 1, we present the function `LeafTransform` which is denotes the LTR operation handling the transformation of raw user data records including user and transformation salts. First, the function generates the salted transform leaf value φ^0 and its associated witness Ω_{LT} based on the compiled circuit for leaf transform \mathcal{L}^s which is parametrized by $\theta_{\mathcal{L}^s}$. The function stores the witnesses privately indexed by the hash of salted raw data tuple, the transform salt and the choice of LTR circuit. Finally, the function returns the transformed value φ^0 , the hash of the leaf transform H^{leaf} , transform salt hash H^r and the leaf index \mathcal{N} .

Algorithm 1 Function for Salted Leaf Transformation

```

1: function LEAFTTRANSFORM( $\delta, \mu, \tau, \mathcal{L}^s, \theta_{\mathcal{L}^s}$ )
2:   compute salted leaf transform  $\varphi^0 \leftarrow \mathcal{L}^s([\delta, \mu, \tau]; \theta_{\mathcal{L}^s})$ 
3:   set  $H^{(\delta, \mu)} \leftarrow \text{hash}(\delta, \mu)$  and  $H^r \leftarrow \text{hash}(\tau)$ 
4:   generate witness  $\Omega_{LT} \leftarrow [\delta, \mu, \tau, \varphi^0]$ 
5:    $\triangleright$  store LT witness privately
6:   STOREPRIVATELTWITNESS( $[H^{(\delta, \mu)}, H^r, \mathcal{L}^s], [\Omega_{LT}, \theta_{\mathcal{L}^s}]$ )
7:    $\triangleright$  determine leaf hash and index
8:   set  $H^{leaf} \leftarrow \text{hash}(\varphi^0)$ 
9:   set  $\mathcal{N} \leftarrow \text{Decimal}(H^{leaf})$ 
10:  return  $\varphi^0, H^{leaf}, H^r, \mathcal{N}$ 
10: end function

```

4.2.2 CSMT Construction : The CRO constructs the CSMT using the function `BuildSMT` as represented in Algorithm 2. The function consumes a given user set U with salted leaf transformations and indices denoted by $\{\mathcal{N}_i, \varphi_i^0\}_{u_i \in U}$, a CSMT tree height of K , as well as the aggregation function \mathcal{A}^l parametrized by $\theta_{\mathcal{A}^l}$. The CRO inserts

the non-default user leaves at the appropriate locations while the rest are left with the default value. Using a bottom-up aggregation approach, the CRO builds the sparse Merkle tree by recursively computing the parent for each node identified by its hash using $\mathcal{A}^l(\cdot, \theta_{\mathcal{A}^l})$. The aggregation results in the root value $\Psi^K[0]$, root hash $H^K[0]$ and CSMT witnesses arranged in a sparse Merkle tree format denoted by Ω_{CSMT} . While the CSMT witnesses are stored privates, the function returns the root value and the root hash as their outputs.

Algorithm 2 CSMT Construction

```

1: function BUILDSMT( $\{\mathcal{N}_i, \varphi_i^0\}_{u_i \in U}, K, \mathcal{A}^l, \theta_{\mathcal{A}^l}$ )
2:   set  $\Psi^0[j] \leftarrow \mathcal{L}^s(\emptyset) \forall j \in \{0, 2^K - 1\}$   $\triangleright$  Initialize  $2^K$  leaves
3:    $\triangleright$  insert valid user leaves at their hashed indices
4:    $\Psi^0[\mathcal{N}_i] \leftarrow \varphi_i^0 \forall (\mathcal{N}_i, \varphi_i^0)$ 
5:    $\triangleright$  compute leaf-level hashes
6:    $H^0[j] \leftarrow \text{hash}(\Psi^0[j]) \forall j \in \{0, 2^K - 1\}$ 
7:    $\triangleright$  bottom-up aggregation
8:   for  $k = 1$  to  $K$  do
9:     for  $j = 0$  to  $2^{K-k} - 1$  do
10:     $\varphi_L^k \leftarrow \Psi^{k-1}[2j]$ 
11:     $\varphi_R^k \leftarrow \Psi^{k-1}[2j + 1]$ 
12:    compute parent aggregate  $\Psi^k[j] \leftarrow \mathcal{A}^l(\varphi_L^k, \varphi_R^k; \theta_{\mathcal{A}^l})$ 
13:    compute parent hash  $H^k[j] \leftarrow \text{hash}(\Psi^k[j])$ 
14:   end for
15:   end for
16:    $\triangleright$  construct CSMT Witness object for membership tests
17:    $\Omega_{CSMT} \leftarrow \left[ \{\Psi^k[j]\}_{j=0}^{2^{K-k}-1} \right]_{k=0}^K$ 
18:   STOREPRIVATECSMTWITNESS( $\mathcal{A}^l, (\Omega_{CSMT}, \theta_{\mathcal{A}^l})$ )
19:    $\triangleright$  return global aggregate, root hash and CSMT witness
20:   return  $\Psi^K[0], H^K[0]$ 
20: end function

```

4.2.3 Generation of LTR Proofs : In function `CRO-LTRProve` given in Algorithm 3, we discuss the mechanism to generate zk-SNARKs for the leaf transformation on raw user data records. The function consumes the hashes of salted raw user data and the transform salts denoted by $H^{(\delta, \mu)}, H^r$ respectively. Additionally the verification key $vk_{\mathcal{L}^s}$ for the specific leaf transformation function must also be provided to help identify the specific transformation function for which the proofs are being requested. Consequently, the function loads the corresponding proving key $pk_{\mathcal{L}^s}$, the compiled circuit \mathcal{L}^s . Next, the the LTR witnesses and parameters $\Omega_{LT}, \theta_{\mathcal{L}^s}$ are looked up based on the provided salted raw user data record and transform salts. As a result, the CRO generates the zk-SNARK $\Pi_{\mathcal{L}^s}$ and returns the leaf hash, index and the SNARK artifact denoted by H^{leaf}, \mathcal{N} and $\Pi_{\mathcal{L}^s}$ respectively.

4.2.4 Generation of MRP Proofs : The mechanism for generating MRP proofs for a given leaf transform of user data is denoted by the function `CRO-MRPProve` which is presented in Algorithm 4. The function consumes the leaf hash and index H^{leaf}, \mathcal{N} , a nonce value

Algorithm 3 Salted Leaf Transform Proof Generation

```

1: function CRO-LTRPROVE( $H^{(\delta, \mu)}$ ,  $H^\tau$ ,  $vk_{\mathcal{L}^s}$ )
2:   load compiled circuit  $\mathcal{L}^s$  based on verification key  $vk_{\mathcal{L}^s}$ 
3:   load proving keys  $pk_{\mathcal{L}^s}$  based on  $\mathcal{L}^s$ 
4:   ▷ load the LTR witness and parameters
5:    $(\Omega_{LT}, \theta_{\mathcal{L}^s}) \leftarrow \text{LOADPRIVATELTWITNESS}(H^{(\delta, \mu)}, H^\tau, \mathcal{L}^s)$ 
6:   ▷ generate LTR zk-SNARK
7:    $\Pi_{\mathcal{L}^s} \leftarrow \text{Prove}(pk_{\mathcal{L}^s}, \mathcal{L}^s, \theta_{\mathcal{L}^s}, \Omega_{LT})$ 
8:   determine leaf hash  $H^{leaf} \leftarrow \Pi_{\mathcal{L}^s}[\text{output}]$ 
9:   compute leaf index  $\mathcal{N} \leftarrow \text{Decimal}(H)$ 
10:  ▷ return leaf transform, hash, index and proof artifact
11:  return  $H^{leaf}, \mathcal{N}, \Pi_{\mathcal{L}^s}$ 
12: end function

```

η supplied by the verifier as well as the verification key $vk_{\mathcal{A}^l}$ to identify the aggregation circuit and parameters. The leaf index is binarized to represent an array of selector or path index bits to help serve as a route from the corresponding leaf to the root of the CSMT. The nonce value plays an important role to help assert the integrity of the per-hop MRP zk-SNARK artifacts with respect to the binary representation of the leaf node index obtained from the LTR proof.

After loading the proving key, $pk_{\mathcal{A}^l}$, aggregator circuit \mathcal{A}^l and the CSMT witness and parameters $(\Omega_{CSMT}, \theta_{\mathcal{A}^l})$, the function iterates through all levels of the tree starting from leaf level. At each iteration, the parent value Ω_{CSMT}^P is obtained from CSMT witness object, and depending on the corresponding path index bit, the orientation (i.e. left or right of the current node) of the sibling is decided. Based on the witnesses, k^{th} -hop zk-SNARK is generated which is denoted by $\Pi_{\mathcal{A}^l}^{(k)}$. The function returns the hash of the root H^{root} , the series of zk-SNARK artifacts for each hop denoted by Π_{CSMT}^u as well as the array of path index bits B .

4.2.5 Integrated CoMeTIC CRO Logic : We combine the algorithmic components discussed above into a standalone function denoted by CosmeticCROBuild as presented in Algorithm 5. Without loss of generality, we consider a PHR database with an exhaustive user base U such that $U^{inc} \subseteq U$ represents the set of users chosen to participate in the user study. The function CosmeticCROBuild consumes U, U^{inc} in addition to verification keys $vk_{\mathcal{L}^s}, vk_{\mathcal{A}^l}$ for LTR and MRP proofs to identify the relevant aggregation and leaf transform functions respectively. The function acquires the raw salted user data set based on U and carries out a leaf transform using LeafTransform, assigning a unique randomized transform salt to each user. Consequently, the function invokes BuildSMT using the selected group of users U^{inc} to yeild the root value and root hash denoted by Ψ^{root}, H^{root} . Finally, the CRO distributes the hash of transform salt of each user H_u^τ and the verification keys $vk_{\mathcal{L}^s}, vk_{\mathcal{A}^l}$ corresponding to the transform and aggregation functions. We note that even though Algorithm 5 considers all users in the PHR database for effecting the leaf transforms, doing so is not necessary and is presented as such for representational convenience and to highlight the generation of both inclusion and exclusion proofs in later sections.

Algorithm 4 CSMT Merkle Path Proof Generation

```

1: function CRO-MRPPROVE( $H^{leaf}$ ,  $\mathcal{N}, \eta, vk_{\mathcal{A}^l}$ )
2:   initialize empty hop-proof list  $\Pi_{CSMT}$ 
3:   load compiled circuit  $\mathcal{A}^l$  based on verification key  $vk_{\mathcal{A}^l}$ 
4:   load proving keys  $pk_{\mathcal{A}^l}$  based on  $\mathcal{A}^l$ 
5:   ▷ load the CSMT witness and parameters
6:    $(\Omega_{CSMT}, \theta_{\mathcal{A}^l}) \leftarrow \text{LOADPRIVATECSMTWITNESS}(\mathcal{A}^l)$ 
7:   compute binary index path  $B \leftarrow \text{Bin}(\mathcal{N})$ 
8:   set starting index to be  $j \leftarrow \mathcal{N}$  which is the leaf index
9:   ▷ iterate through CSMT levels
10:  for  $k = 0$  to  $K$  do
11:    set parent index  $p \leftarrow \text{Floor}(j/2)$ 
12:    obtain parent node value  $\Omega_{CSMT}^P \leftarrow \Omega_{CSMT}[p, k]$ 
13:    ▷ identify MRP hop witness
14:    if  $B[k] = 0$  then ▷ current node is left sibling
15:      set  $\Omega_{CSMT}^k = \{\Omega_{CSMT}[j, k], \Omega_{CSMT}[j+1, k], \Omega_{CSMT}^P\}$ 
16:    else ▷ current node is right sibling
17:      set  $\Omega_{CSMT}^k = \{\Omega_{CSMT}[j-1, k], \Omega_{CSMT}[j, k], \Omega_{CSMT}^P\}$ 
18:    end if
19:    ▷ generate MRP hop zk-SNARK
20:     $\Pi_{\mathcal{A}^l}^{(k)} \leftarrow \text{Prove}(pk_{\mathcal{A}^l}, \mathcal{A}^l, \theta_{\mathcal{A}^l}, \Omega_{CSMT}^k, B[k], \eta)$ 
21:    append  $\Pi_{\mathcal{A}^l}^{(k)}$  to  $\Pi_{CSMT}$ 
22:  end for
23:  ▷ set last hash as CSMT root
24:   $H^{root} \leftarrow H_P^k$ 
25:  ▷ return root hash, CSMT proofs
26:  return  $H^{root}, \Pi_{CSMT}^u, B$ 
27: end function

```

4.3 Verifier Oriented Algorithmic Components

The algorithmic components on the Verifier are in charge of validating zk-SNARKs delivered by the CRO as a means to certify the inclusion of individual user datum consistent with the claimed leaf transform and aggregation functions. We note that the Verifier side logic is purely driven by the exchange of zk-SNARKs and the hash derivatives contained therein. We subdivide the entire task set into three different algorithmic components each pertaining to verifying individual LTR, and per-hop MRP zk-SNARKs, as well as validating inclusion proofs in the CRO CSMT. The same algorithmic structure provides support for both inclusion and exclusion proofs in the CoMeTIC algorithmic framework. For brevity, in this section, we only discuss the main verifier logic represented in Algorithms 7 and 7 that relies on the primitives LTRVerify and MRPHopVerify, each of which have been discussed at length in Appendix E.1.

In Algorithm 6 we present the VerInc function that relies on the hashes of the salted raw user data record $H^{(\delta_u, \mu_u)}$, the user specific leaf transform H_u^{leaf} , CSMT root H^{root} and the nonce H^η in addition to the set of LTR and MRP zk-SNARK artifacts and their corresponding verification keys denoted by $\Pi^u, vk_{\mathcal{L}^s}, vk_{\mathcal{A}^l}$

Algorithm 5 CRO Component of CoSMETIC

```

1: function COSMETICCROBUILD( $U, U^{inc}, \mathbf{vk}_{\mathcal{L}^s}, \mathbf{vk}_{\mathcal{A}^l}$ )
2:  acquire user set  $U$ , salted raw data  $\Delta_U^s$ , transform salt array
    $T_U$  from PHR database
      ▷ load LTR and MRP proof generation artifacts
3:  load compiled circuits  $\mathcal{L}^s, \mathcal{A}^l$  and parameters  $\theta_{\mathcal{L}^s}, \theta_{\mathcal{A}^l}$ 
      ▷ build CSMT
4:  for  $u \in U$  do
5:   acquire  $(\delta_u, \mu_u) \in \Delta_U^s$ 
6:   acquire transform salt  $\tau_u$  for user  $u$  from  $T_U$ 
7:    $\varphi_u^0, H_u^{leaf}, H_u^\tau, \mathcal{N}_u \leftarrow \text{LEAFTRANSFORM}(\delta_u, \mu_u, \tau_u, \mathcal{L}^s, \theta_{\mathcal{L}^s})$ 
8:  end for
      ▷ build SMT based on included user set  $U^{inc}$  in clinical study
9:   $\Psi^{root}, H^{root} \leftarrow \text{BUILD SMT}(\{\mathcal{N}_u, \varphi_u^0\}_{u \in U^{inc}}, K, \mathcal{A}^l, \theta_{\mathcal{A}^l})$ 
      ▷ send transform salt hash and verification keys to users
10:  distribute  $[H_u^\tau]$  for all users  $u \in$  user set  $U$ 
11:  publish  $H^{root}, \mathbf{vk}_{\mathcal{L}^s}, \mathbf{vk}_{\mathcal{A}^l}$  publicly
12:  return  $\Psi^{root}, H^{root}$ 
13: end function

```

respectively. The function enables the verification of the LTR zk-SNARK using the LTRVerify function. Next, we begin the process of verifying the MRP zk-SNARK artifacts by considering the binary path representation of H_u^{leaf} . We iterate over each hop of the CSMT starting from the leaf level with H_u^{leaf} all the way to the root. At each level, we retrieve the right and left input hashes from the per-hop CSMT proof artifact represented by $\Pi_{\mathcal{A}^l}^k$. The right and left inputs are checked for consistency with respect to the selector bit corresponding to the current hop as well as CSMT level. Consequently, we validate the zk-SNARK of the hop using the MRPHopVerify function. Passing the validation criteria for every hop as well as the leaf transformation results in a successfully verifying the inclusion of a specific user's data in the clinical study.

We provide Algorithm 7 to summarize the algorithmic design at the verifier end. In Algorithm 7, the verifier invokes CRO-LTRProve and CRO-MRPProve functions on the CRO. These CRO based functions can be implemented as an RPC call or a REST API functionality. The verifier then tests the inclusion using the function VerInc. Consistency of the selector bit path and the salted leaf transformation reported by CRO-MRPProve and CRO-LTRProve is critical to ensure that the generated proofs pertain to the same user datum. Additionally a successful outcome of the VerInc function results concludes the verification process at the verifier.

4.4 Security Model and Guarantees

There are two fundamental formal guarantees that the CoSMETIC framework delivers with respect to the CRO. First, using Proposition 1, it establishes the CSMT architecture, providing necessary and sufficient conditions to evaluate the membership of a particular user's data in a reduction operation. Second, Proposition 2 formally proves that successful verification of LTR and MRP zk-SNARKS are necessary and sufficient to realize the membership function. Lastly,

Algorithm 6 Function for CSMT Inclusion Verification

```

1: function VERINC( $H^{(\delta_u, \mu_u)}, H^\tau, H_u^{leaf}, \Pi^u, H^{root}, H^\eta, \mathbf{vk}_{\mathcal{L}^s}, \mathbf{vk}_{\mathcal{A}^l}$ )
2:  extract  $\Pi_{\mathcal{L}^s}^u$  from  $\Pi^u$  and  $\Pi_{\mathcal{A}^l}^{u,1:K}$  from  $\Pi^u$ 
3:   $\Phi_{\mathcal{L}^s}^u \leftarrow \text{LTRVERIFY}(\mathbf{vk}_{\mathcal{L}^s}, \Pi_{\mathcal{L}^s}^u, H^{(\delta_u, \mu_u)}, H^\tau, H_u^{leaf})$ 
4:  if  $\Phi_{\mathcal{L}^s}^u = 0$  then                                ▷ LTR cannot be verified
5:   return False
6:  end if
7:  set binary path  $B \leftarrow H_u^{leaf}$ 
8:  set  $H^{curr} \leftarrow H_u^{leaf}$ 
9:  for  $k = 1$  to  $K$  do
10:   retrieve MRP hop proof  $\Pi_{\mathcal{A}^l}^k \leftarrow \Pi_{\mathcal{A}^l}^{u,1:K}[k]$  for level  $k$ 
      ▷ find siblings from MRP hop proof based on selector bit
11:   if  $B[k] = 0$  then
12:     $H^R \leftarrow \Pi_{\mathcal{A}^l}^k[\text{RightInput}]$  and  $H^L \leftarrow H^{curr}$ 
13:   else
14:     $H^L \leftarrow \Pi_{\mathcal{A}^l}^k[\text{LeftInput}]$  and  $H^R \leftarrow H^{curr}$ 
15:   end if
      ▷ verify MRP hop proof
16:    $\Phi_{\mathcal{A}^l}^{u,k} \leftarrow \text{MRPHOPVERIFY}(\mathbf{vk}_{\mathcal{A}^l}, \Pi_{\mathcal{A}^l}^k, H^L, H^R, \text{hash}(B[k]), H^\eta)$ 
17:   if  $\Phi_{\mathcal{A}^l}^{u,k} = 0$  then                                ▷ MRP cannot be verified
18:    return False
19:   end if
      ▷ set the MRP hop output as current value
20:    $H^{curr} \leftarrow \Pi_{\mathcal{A}^s}[\text{Parent}]$ 
21:  end for
      ▷ check root hash and selector path and leaf hash consistency
22:  if  $H^{curr} = H^{root}$  and  $\text{Decimal}(B) = H_u^{leaf}$  then
23:   return True
24:  else                                              ▷ inconsistent proving system
25:   return False
26:  end if
27: end function

```

Algorithm 7 Verifier Component of CoSMETIC

```

1: function COSMETICVERIFIER( $u$ )
2:  load  $H^{(\delta, \mu)}$  pertaining to user  $u$  from PHR database
      ▷ received during proof generation
3:  load  $H^\tau, \mathbf{vk}_{\mathcal{L}^s}, \mathbf{vk}_{\mathcal{A}^l}$  sent by CRO
      ▷ invoke LTR prover remotely on CRO
4:   $H^{leaf}, \mathcal{N}, \Pi_{\mathcal{L}^s} \leftarrow \text{CRO-LTRPROVE}(H^{(\delta, \mu)}, H^\tau, \mathbf{vk}_{\mathcal{L}^s})$ 
      ▷ invoke MRP prover remotely on CRO
5:   $H^{root}, \Pi_{\mathcal{A}^l}, B \leftarrow \text{CRO-MRPPROVE}(H^{leaf}, \mathcal{N}, \eta, \mathbf{vk}_{\mathcal{A}^l})$ 
6:  consolidate LTR and MRP proofs  $\Pi^u \leftarrow \{\Pi_{\mathcal{L}^s}, \Pi_{\mathcal{A}^l}\}$ 
7:   $\Phi^{(\delta, \mu)} \leftarrow \text{VERINC}(H^{(\delta, \mu)}, H^{leaf}, \Pi^u, H^{root}, H^\eta, \mathbf{vk}_{\mathcal{L}^s}, \mathbf{vk}_{\mathcal{A}^l})$ 
8:  if  $\Phi^{(\delta, \mu)} = 0$  then
9:   inclusion verification failed
10:  end if
11: end function

```

the algorithmic foundations of the CoSMeTIC framework are driven largely by Assumptions 1 - 3 which serve as necessary conditions for a successful and secure implementation of the framework.

From the algorithmic implementation standpoint, there are exactly two potential gaps where an incorrect evaluation of the membership function cannot be detected solely on the basis of Proposition 2. The first gap pertains to the soundness of knowledge argument afforded by zk-SNARKs which inhibits the practical likelihood of obtaining proof artifacts consistent with Proposition 2 but generated using incorrect witnesses. The second gap focuses on the data exclusivity argument which pertains to the ability to exclusively commit to the set of users whose data was included in a particular reduction operation. The data exclusivity argument is an essential security component to prove the tamper-resistant aspects of the dataset used for the clinical study.

4.4.1 Knowledge Soundness : Our knowledge soundness argument is based on the implementation mechanisms for verification highlighted in Algorithm 7. As a consequence, we establish Proposition 3 which provides formal guarantees pertaining to the knowledge soundness of the zk-SNARK artifacts.

PROPOSITION 3. *The knowledge-soundness property of the underlying zero knowledge system guarantees that the membership (or non-membership) of user u for the reduction operation $R(\mathcal{A}, \mathcal{L}, U^{inc})$ can be violated with only negligible probability.*

PROOF. Proof given in Appendix C.3 \square

Fundamentally, the proposition explores the ability for such a CRO to use incorrect LTR witnesses, inconsistent leaf indices or manipulated MRP proof artifacts for one or more hops as a means to generate zk-SNARKs that can be verified using Algorithm 7. Using the argument of knowledge-soundness of the Halo2 proving background, Proposition 3 argues that a compromised CRO cannot practically use incorrect witnesses to generate zk-SNARK artifacts.

4.4.2 Data Exclusivity : To demonstrate the data exclusivity argument, we consider $U^{inc} \subseteq U$ as having been the set of users whose data a compromised CRO claims to use for its clinical study while actually utilizing \hat{U}^{inc} with $\hat{U}^{inc} \cap U^{inc} \neq \emptyset$. We formally define data exclusivity argument in Definition 8.

DEFINITION 8. *Given membership function \mathcal{M} and a reduction function R , a clinical study is deemed to be data exclusive to a set of users $U^{inc} \subseteq U$ if and only if the following conditions hold*

$$\#u \in U^{inc} \text{ and } \mathcal{M}([u, \delta_u] | R) = 1,$$

where δ_u is the raw user data record for any user u .

Based on Definition 8 we derive necessary conditions for data exclusivity as presented in Proposition 4. A prerequisite for Proposition 4 is to check the provenance of the leaves by ensuring that every non-default leaf must be the result of a leaf transform on a raw data record that belongs to a PHR database. However, verifying the provenance of each leaf is trivial and straightforward based on Algorithm 9.

PROPOSITION 4. *Given a set of users U with corresponding ordered salted leaf transformed set denoted by $\Delta_U^{\mathcal{L}^s}$, data exclusivity is guaranteed if the ordered leaf set corresponding to every subtree rooted at a non-default, non-leaf is a subset of $\Delta_U^{\mathcal{L}^s}$.*

PROOF. Proof given in Appendix C.4 \square

Proposition 3 provides the set of criteria which can be used by the CRO to prove data exclusivity based on analyzing the set of non-default leaves that appear across the entire CSMT. We note however that to implement Proposition 4 the CRO would have to divulge the LTR and MRP zk-SNARKs of all users that are part of the set U^{inc} whose data was included in the clinical study. In Appendix C.5, we provide a detailed discussion for strategies that can successfully detect violations in data exclusivity including Algorithm 8 which outlines an implementation mechanism for checking the provenance and data exclusivity of a particular reduction operation.

5 Experimental Results

We present the computational experiments for evaluating CoSMeTIC using three real world clinical case studies that are driven by two distinct clinical datasets. All experiments were conducted on a virtual machine (VM) running Ubuntu 24.04, provisioned with 16 vCPUs and 100 GB of RAM. The implementation was carried out in Python 3.11, with model inference performed using PyTorch 2.7.1. Zero-knowledge proofs were generated using the ezkl library, which underlies the zkSNARK construction within the CoSMeTIC framework. All experiments were evaluated under multiple fixed-point precision configurations, controlled by the scale parameter. We consider scales of 8, 10, 12, and 14, which directly determine the arithmetic precision inside the zero-knowledge circuits. This range allows us to evaluate the impact of increasing cryptographic precision on performance, numerical stability, and cryptographic overhead.

5.1 Clinical Case Studies

We evaluate CoSMeTIC across three representative statistical workflows commonly encountered in clinical and genomic studies that pertain to the Kolmogorov-Smirnov (KS) test, the Logistic Likelihood-Ratio Test (LR), and the Logistic Accuracy (ACC) test. Our evaluation focuses on three distinct dimensions involving the cost of circuit compilation and witness generation, the stability of the resulting statistical outputs and the cryptographic overhead incurred through proving and verification keys. Together, these metrics characterize the practicality of deploying CoSMeTIC in privacy-sensitive analytical pipelines.

Case Study Datasets: To drive the case studies, we utilize datasets from two real-world cases pertaining to Huntington's disease (HD) and immunodeficiency virus type 1 (HIV-1) with more details on each disease provided in Appendix D.1.1 and D.1.2 respectively. For Huntington's we evaluate whether the distribution of Cytosine–Adenine–Guanine (CAG) repeat lengths differs between individuals with clinical HD and healthy controls. Two independent cohorts are constructed, each comprising 50 individuals, representing the healthy and HD groups. A two-sample KS test is implemented using the CoSMeTIC framework applied to assess distributional differences between both the groups. In the second case study related to HIV-1, we examine the Env-targeting therapeutic BMS-626529 (Temsavir, TMR) [26, 45]. We analyze a dataset of 12 samples from distinct HIV-infected individuals. Each sample was associated with four features that describe the amino acid sequence at the above Env positions, and a resistance value measured in vitro using the

PhenoSense GT assay. Using the CoSMETIC framework, we implement a Likelihood Ratio Test (LRT) to compare a full versus reduced logistic regression model using training data and then compute the accuracy (Acc) for a set of patients in the test set. The architecture of the CSMT within the CoSMETIC framework for the KS, LR and Acc tests has been illustrated in Figure 4 presented in Appendix E.

EZKL Scale	Model 1		Model 2		Total Time	
	Circuit Witness		Circuit Witness			
	PK	VK	PK	VK		
8	307.53	1070.87	292.40	1082.41	2916.16	
10	303.07	1063.42	306.40	1070.08	2867.4	
12	301.02	1069.79	299.44	1078.96	2874.8	
14	291.00	1080.10	307.74	1081.95	2892.24	

Table 1: KS circuit and witness generation time (seconds) across EZKL scales

EZKL Scale	Full Model		Reduced Model		Total Time	
	Circuit Witness		Circuit Witness			
	PK	VK	PK	VK		
8	297.63	971.44	293.57	975.65	2641.62	
10	267.61	883.93	271.59	880.93	2394.99	
12	270.30	887.07	258.56	869.07	2459.20	
14	274.54	888.47	276.65	896.43	2523.01	

Table 2: LRT circuit and witness generation time (seconds) across EZKL scales

EZKL Scale	Length		Accuracy		Total Time	
	Circuit Witness		Circuit Witness			
	PK	VK	PK	VK		
8	343.72	1181.16	323.31	1163.35	3011.54	
10	341.87	1171.05	292.86	1154.64	2960.42	
12	345.77	1080.57	324.30	1122.04	2872.68	
14	347.23	1089.28	325.69	1178.08	2940.28	

Table 3: ACC circuit and witness generation time (seconds) across EZKL scales

EZKL Scale	KS Max Gap	LRT Statistic	ACC Accuracy
8	0.999	386.78	0.749
10	0.999	386.78	0.749
12	0.999	386.78	0.749
14	0.999	386.78	0.749
No Scale	0.999	386.78	0.749

Table 4: Stability of statistical outputs across EZKL precision scales

5.2 Case Study Results

We present the results of our case studies in terms of the witness generation times as well as the computational system performance of the end-to-end LTR and MRP proving mechanism for KS, LR and ACC Tests. We present the proving and verification keys sizes for each case study in Appendix F.

EZKL Scale	Max Gap			LRT Statistic		
	PK	VK	Time	PK	VK	Time
8	13.24	3.07	162.95	10.29	2.43	103.31
10	13.24	3.07	124.43	10.29	2.43	125.65
12	13.24	3.07	125.59	10.29	2.43	174.20
14	13.24	3.07	131.45	10.29	2.43	186.93

Table 5: KS and LRT statistics Proving(GB), verification(MB) and generation time (seconds) key sizes across EZKL Scale

5.2.1 *Kolmogorov-Smirnov (KS) Test* : As reported in Table 1, circuit compilation and witness generation times remain tightly bounded across all EZKL Scale configurations. Increasing arithmetic precision introduces only minor fluctuations in total generation time, indicating that higher fixed-point precision does not significantly impact the computational cost of the KS workflow. More importantly, the computed max-gap statistic remains invariant across all precision settings. This invariance demonstrates that increasing zero-knowledge precision does not distort the underlying non-parametric hypothesis test, confirming that CoSMETIC preserves numerical correctness under cryptographic constraints.

5.2.2 *Logistic Likelihood-Ratio (LRT) Test* : As shown in Table 2, both circuit and witness generation times remain stable as the EZKL Scale increases. Despite higher arithmetic precision, the LR statistic is preserved exactly across all configurations, demonstrating that CoSMETIC maintains numerical fidelity for parametric hypothesis testing under zero-knowledge constraints. This property is particularly important in regulated settings, where even small numerical deviations can affect downstream clinical or regulatory decisions.

5.2.3 *Logistic Accuracy (ACC) Test* : As reported in Table 3, both transformers incur relatively modest circuit and witness generation times compared to the KS and LRT workflows. Across all EZKL Scale values, the observed classification accuracy remains unchanged, indicating that zero-knowledge proof construction does not interfere with model evaluation outcomes. Moreover, we notice that the total generation times vary only slightly with increasing precision, suggesting predictable performance behavior. This confirms that repeated accuracy verification can be supported efficiently within the CoSMETIC framework.

Across all evaluated statistical workflows, CoSMETIC demonstrates strong scalability and numerical stability with increasing zero-knowledge precision. Specifically, we observe stability in circuit and witness generation times across diverse scale values while preserving exact statistical outputs. These results collectively confirm that CoSMETIC enables privacy-preserving statistical inference without compromising numerical correctness or cryptographic scalability.

System-level CPU utilization: Figures 2(a)–2(c) show the prover CPU utilization during KS, LRT, and ACC proof generation, respectively. For the KS test (Figure 2(a)), CPU usage exhibits periodic fluctuations, reflecting alternating computation phases associated with histogram aggregation and cumulative distribution comparison within the KS circuit. Despite these fluctuations, overall CPU utilization remains consistently elevated, indicating sustained computational activity throughout the proving process.

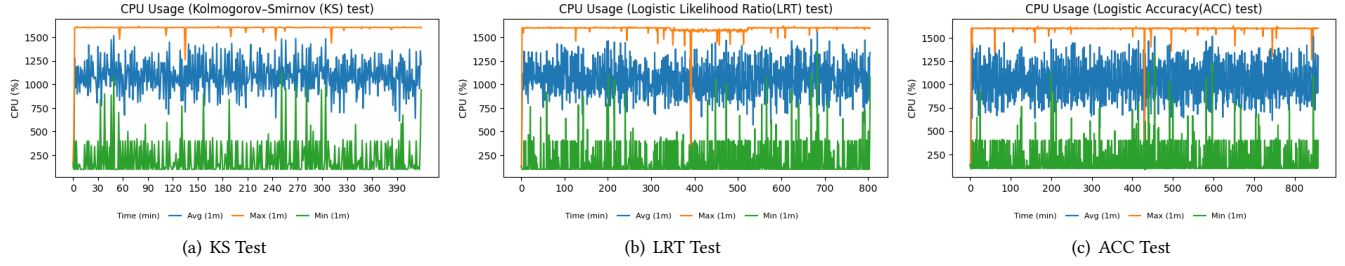


Figure 2: Prover CPU utilization during KS, LRT, and ACC proof generation.

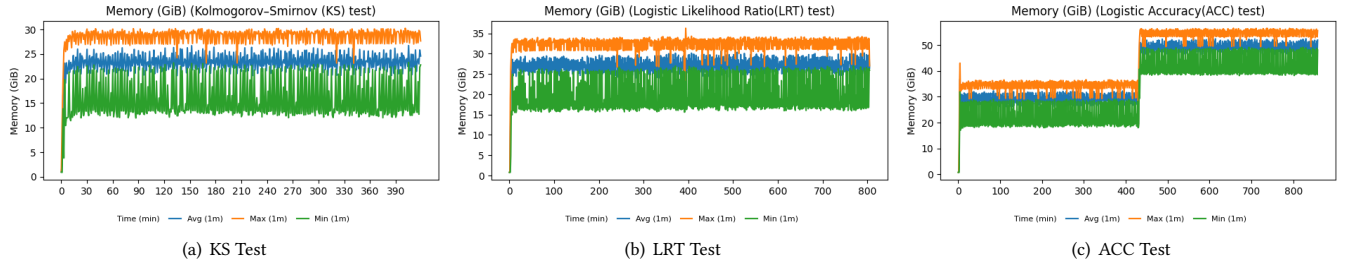


Figure 3: Prover memory utilization during KS, LRT, and ACC proof generation.

The LRT workload (Figure 2(b)) demonstrates a more uniform CPU utilization profile, corresponding to continuous arithmetic computation required to evaluate both the full and reduced logistic regression models within the zero-knowledge circuit. The absence of pronounced oscillations suggests a steady, compute-bound execution pattern.

Similarly, the ACC workflow (Figure 2(c)) shows sustained CPU utilization across the entire execution window, indicating continuous computation during both the length SMT proof phase and the subsequent accuracy proof phase. The lack of extended idle periods suggests that ACC proof generation maintains a stable computational workload across phases.

System-level memory utilization. Figures 3(a)–3(c) present the prover memory utilization during KS, LRT, and ACC proof generation. For the KS test (Figure 3(a)), memory usage remains stable throughout execution, with minimal divergence between minimum, average, and maximum values. This behavior indicates that KS proof generation relies on a fixed working set after initialization and does not require repeated large memory allocations.

In the LRT case (Figure 3(b)), memory utilization also exhibits a steady profile with limited variation over time. The absence of large memory spikes suggests efficient reuse of intermediate buffers during witness generation and likelihood computation.

For the ACC workflow (Figure 3(c)), memory usage remains stable during the initial execution period and increases when the system transitions from length SMT proof generation to accuracy proof generation. After this transition, memory utilization stabilizes at a higher level, indicating predictable, phase-dependent memory usage rather than unbounded allocation growth.

6 Conclusion

In this paper, we introduce CoSMETIC, a zero-knowledge framework based on Computational Sparse Merkle Trees (CSMTs) that enables verifiable statistical computation while preserving patient privacy in clinical research. By leveraging Merkle tree structure and computational reduction operations, CSMTs support succinct inclusion and exclusion proofs for individual users whose data participate in specific stages of a statistical analysis. CoSMETIC integrates zk-SNARKs to provide end-to-end, publicly verifiable guarantees of data membership and exclusion across the computational pipeline. We formalize soundness conditions for these proofs using state-of-the-art proving systems such as Halo2 and demonstrate that CoSMETIC can also verify claims of exclusive data usage from subsets of large medical databases. Through diverse real-world case studies, we show that the framework is extensible to a wide range of statistical methods used in clinical research.

To evaluate CoSMETIC, we design three representative use cases using real-world clinical data from Huntington’s disease (HD) and HIV-1 studies. First, we implement a two-sample Kolmogorov-Smirnov (KS) test to verify whether CAG repeat length distributions differ between HD patients and healthy controls, while proving that only approved cohort data were used and all non-participants were excluded. Second, we construct a publicly verifiable likelihood ratio test (LRT) for HIV-1 resistance to Temsavir using nested logistic-regression models to assess the significance of selected genomic features. Third, we extend the framework to support verifiable evaluation of predictive accuracy under the same inclusion and exclusion guarantees. Across multiple zero-knowledge scales, we demonstrate that circuit and witness generation times,

statistical outputs, and key sizes remain practical and stable, showing that privacy-preserving hypothesis testing can be achieved without sacrificing computational efficiency or statistical validity.

Finally, we show that CoSMETIC enables regulators to verify the authenticity and correct use of datasets underlying clinical studies, while allowing participants to obtain publicly verifiable proofs of data inclusion or exclusion. By combining correctness, privacy, and transparency, CoSMETIC offers a practical and scalable foundation for trustworthy, auditable, and privacy-preserving clinical research.

Acknowledgments

Funding Support: This material is based upon work supported by the National Science Foundation (NSF) under Grant No. 2348411 and by National Institutes of Health (NIH) grant R01 AI170205.

Generative AI Usage: Generative AI tools such as ChatGPT were used for editorial purposes in the preparation of this manuscript (e.g., grammar refinement, stylistic polishing, and clarity improvements). The authors relied on generative AI tools for assisting with the creation of skeletal code for some class and function declarations as well as for routine debugging activities for the core programming logic. All AI-assisted content was reviewed, verified, and validated by the authors, including re-running experiments and checking citations.

References

- [1] Judith A Aberg, Bronagh Shepherd, Marcia Wang, Jose V Madruga, Fernando Mendo Urbina, Christine Katlama, Shannon Schrader, Joseph J Eron, Princy N Kumar, Eduardo Sprinz, Margaret Gartland, Shiven Chabria, Andrew Clark, Amy Pierce, Max Lataillade, and Allan R Tenorio. 2023. Week 240 efficacy and safety of fostemsavir plus optimized background therapy in heavily treatment-experienced adults with HIV-1. *Infect. Dis. Ther.* 12, 9 (Sept. 2023), 2321–2335.
- [2] Luning Bi, Mohammad Fili, and Guiping Hu. 2022. COVID-19 forecasting and intervention planning using gated recurrent unit and evolutionary algorithm. *Neural Comput. Appl.* 34, 20 (May 2022), 17561–17579.
- [3] Tashrif Billah, Kang Il K Cho, Owen Borders, Yoonho Chung, Michaela Ennis, Grace R Jacobs, Einat Liebenthal, Daniel H Mathalon, Dheshan Mohandass, Spero C Nicholas, Ofer Pasternak, Nora Penzel, Habiballah Rahimi Eichi, Phillip Wolff, Alan Anticevic, Kristen Laulette, Angela R Nunez, Zailyn Tamayo, Kate Buccilli, Beau-Luke Colton, Dominic B Dwyer, Larry Hendricks, Hok Pan Yuen, Jessica Spark, Sophie Tod, Holly Carrington, Justine T Chen, Michael J Coleman, Cheryl M Corcoran, Anastasia Haider, Omar John, Sinead Kelly, Patricia J Marcy, Priya Matneja, Alessia McGowan, Susan E Ray, Simone Veale, Inge Winter-Van Rossum, Jean Addington, Kelly A Allott, Monica E Calkins, Scott R Clark, Ruben C Gur, Michael P Harms, Diana O Perkins, Kosha Ruparel, William S Stone, John Torous, Alison R Yung, Eirini Zoupou, Paolo Fusar-Poli, Vijay A Mittal, Jai L Shah, Daniel H Wolf, Guillermo Cecchi, Tina Kapur, Marek Kubicki, Kathryn Eve Lewandowski, Carrie E Bearden, Patrick D McGorry, René S Kahn, John M Kane, Barnaby Nelson, Scott W Woods, Martha E Shenton, Accelerating Medicines Partnership® Schizophrenia (AMP® SCZ), Justin T Baker, and Sylvain Bouix. 2025. Enabling FAIR data stewardship in complex international multi-site studies: Data Operations for the Accelerating Medicines Partnership® Schizophrenia Program. *Schizophrenia (Heidelberg)* 11, 1 (April 2025), 55.
- [4] Artem Chystiakov, Oleh Komendant, and Kyrylo Riabov. 2025. Cartesian Merkle Tree. arXiv preprint arXiv:2504.10944. <https://arxiv.org/abs/2504.10944>
- [5] James Curzon, Tracy Ann Kosa, Rajen Akalu, and Khalil El-Khatib. 2021. Privacy and Artificial Intelligence. *IEEE Transactions on Artificial Intelligence* 2, 2 (2021), 96–108. doi:10.1109/TAI.2021.3088084
- [6] Jeffrey Dean and Sanjay Ghemawat. 2008. MapReduce: simplified data processing on large clusters. *Commun. ACM* 51, 1 (2008), 107–113.
- [7] Jack J Dongarra, Steve W Otto, Marc Snir, David Walker, et al. 1995. An introduction to the MPI standard. *Commun. ACM* 18, 11 (1995).
- [8] Gregory Falco, Ben Shneiderman, Julia Badger, Ryan Carrier, Anton Dahbura, David Danks, Martin Eling, Alwyn Goodloe, Jerry Gupta, Christopher Hart, Marina Jirotna, Henric Johnson, Cara LaPointe, Ashley J Llorens, Alan K Mackworth, Carsten Maple, Sigurður Ó Emil Pálsson, Frank Pasquale, Alan Winfield, and Zee Kin Yeong. 2021. Governing AI safety through independent audits. *Nat. Mach. Intell.* 3, 7 (July 2021), 566–571.
- [9] Food, Drug Administration, et al. 2024. Evaluating inclusion and exclusion criteria in clinical trials. In *Workshop Report*. [online]. Accessed, Vol. 13.
- [10] Sarah L Gardiner, Martine J van Belzen, Merel W Boogaard, Willeke M C van Roos-Mom, Maarten P Rozing, Albert M van Hemert, Johannes H Smit, Aartjan T F Beekman, Gerard van Grootenhuis, Robert A Schoevers, Richard C Oude Voshaar, Raymund A C Roos, Hannie C Comijs, Brenda W J H Penninx, Roos C van der Mast, and N Ahmad Aziz. 2017. Huntington gene repeat size variations affect risk of lifetime depression. *Transl. Psychiatry* 7, 12 (Dec. 2017), 1277.
- [11] Margaret Gartland, Eric Arnoult, Brian T Foley, Max Lataillade, Peter Ackerman, Cyril Llamoso, and Mark Krystal. 2021. Prevalence of gp160 polymorphisms known to be related to decreased susceptibility to temsavir in different subtypes of HIV-1 in the Los Alamos National Laboratory HIV Sequence Database. *J. Antimicrob. Chemother.* 76, 11 (Oct. 2021), 2958–2964.
- [12] Margaret Gartland, Nannan Zhou, Eugene Stewart, Amy Pierce, Andrew Clark, Peter Ackerman, Cyril Llamoso, Max Lataillade, and Mark Krystal. 2021. Susceptibility of global HIV-1 clinical isolates to fostemsavir using the PhenoSense® Entry assay. *J. Antimicrob. Chemother.* 76, 3 (Feb. 2021), 648–652.
- [13] Brandon Gomes. 2022. SNARKed Merkle Sum Tree: A Practical Proof-of-Solvency Protocol based on Vitalik's Proposal. Ethereum Research forum post. <https://ethresear.ch/t/snarked-merkle-sum-tree-a-practical-proof-of-solvency-protocol-based-on-vitaliks-proposal/14405> Accessed November 2025.
- [14] James F Gusella, Jong-Min Lee, and Marc E McDonald. 2021. Huntington's disease: nearly four decades of human molecular genetics. *Hum. Mol. Genet.* 30, R2 (Oct. 2021), R254–R263.
- [15] Cai Huang, Evan A Clayton, Lilya V Matyunina, L Deette McDonald, Benedict B Benigno, Fredrik Vannberg, and John F McDonald. 2018. Machine learning predicts individual cancer patient responses to therapeutic drugs with high accuracy. *Sci. Rep.* 8, 1 (Nov. 2018), 16444.
- [16] H Jiang, Y M Sun, Y Hao, Y P Yan, K Chen, S H Xin, Y P Tang, X H Li, T Jun, Y Y Chen, Z J Liu, C R Wang, H Li, Z Pei, H F Shang, B R Zhang, W H Gu, Z Y Wu, B S Tang, J-M Burgunder, and Chinese HD Network. 2014. Huntington gene CAG repeat numbers in Chinese patients with Huntington's disease and controls. *Eur. J. Neurol.* 21, 4 (April 2014), 637–642.
- [17] Christopher J Kelly, Alan Karthikesalingam, Mustafa Suleyman, Greg Corrado, and Dominic King. 2019. Key challenges for delivering clinical impact with artificial intelligence. *BMC Med.* 17, 1 (Oct. 2019), 195.
- [18] Michael Kozal, Judith Aberg, Gilles Pialoux, Pedro Cahn, Melanie Thompson, Jean-Michel Molina, Beatriz Grinsztejn, Ricardo Diaz, Antonella Castagna, Princy Kumar, Gulam Latiff, Edwin DeJesus, Mark Gummel, Margaret Gartland, Amy Pierce, Peter Ackerman, Cyril Llamoso, Max Lataillade, and BRIGHTE Trial Team. 2020. Fostemsavir in adults with multidrug-resistant HIV-1 infection. *N. Engl. J. Med.* 382, 13 (March 2020), 1232–1243.
- [19] Oleksandr Kurbatov, Lasha Antadze, Ameen Soleimani, Kyrylo Riabov, and Artem Sdobnov. 2024. IMOK: A Compact Connector for Non-prohibition Proofs to Privacy-Preserving Applications. *IACR Cryptology ePrint Archive* 2024 (2024), 1868. <https://eprint.iacr.org/2024/1868>
- [20] J-M Lee, E M Ramos, J-H Lee, T Gillis, J S Mysore, M R Hayden, S C Warby, P Morrison, M Nance, C A Ross, R L Margolis, F Squitieri, S Orobello, S Di Donato, E Gomez-Tortosa, C Ayuso, O Suchowersky, R J A Trent, E McCusker, A Novello, M Frontali, R Jones, T Ashizawa, S Frank, M H Saint-Hilaire, S M Hersch, H D Rosas, D Luente, M B Harrison, A Zanko, R K Abramson, K Marder, J Sequeiros, J S Paulsen, PREDICT-HD study of the Huntington Study Group (HSG), G B Landwehrmeyer, REGISTRY study of the European Huntington's Disease Network, R H Myers, HD-MAPS Study Group, M E MacDonald, J F Gusella, and COHORT study of the HSG. 2012. CAG repeat expansion in Huntington disease determines age at onset in a fully dominant fashion. *Neurology* 78, 10 (March 2012), 690–695.
- [21] Ruishan Liu, Shemra Rizzo, Samuel Whipple, Navdeep Pal, Arturo Lopez Pineda, Michael Lu, Brandon Arnieri, Ying Lu, William Capra, Ryan Coping, et al. 2021. Evaluating eligibility criteria of oncology trials using real-world data and AI. *Nature* 592, 7855 (2021), 629–633.
- [22] Jorge J Libre-Guerra, Eric M McDade, Suzanne E Schindler, David B Clifford, Charlene Supnet, Alireza Atri, and Randall J Bateman. 2025. Towards pharmacological prevention of Alzheimer disease. *Nat. Rev. Neurol.* 21, 12 (Dec. 2025), 721–733.
- [23] Marie Lonfils. 2023. *Risk-Limiting Audit Optimization with ElectionGuard: Zero-Knowledge Arguments on Chaum-Pedersen Multi-Commitments*. Master's thesis. Université catholique de Louvain, Louvain-la-Neuve, Belgium. <https://thesis.ulb.ac.be/entities/masterthesis/5143cd5c-4284-49e5-9225-72a5f3b9ceb0> Master's thesis.
- [24] M Macdonald. 1993. A novel gene containing a trinucleotide repeat that is expanded and unstable on Huntington's disease chromosomes. *Cell* 72, 6 (March 1993), 971–983.
- [25] Bradley Malin, David Karp, and Richard H Scheuermann. 2010. Technical and policy approaches to balancing patient privacy and data sharing in clinical and translational research. *J. Investig. Med.* 58, 1 (Jan. 2010), 11–18.
- [26] Anthony Markham. 2020. Fostemsavir: First approval. *Drugs* 80, 14 (Sept. 2020), 1485–1490.
- [27] Luis Menéndez-Arias. 2013. Molecular basis of human immunodeficiency virus type 1 drug resistance: overview and recent developments. *Antiviral Res.* 98, 1

(April 2013), 93–120.

[28] Alfred J. Menezes, Paul C. van Oorschot, and Scott A. Vanstone. 1996. *Handbook of Applied Cryptography*. CRC Press.

[29] Nagaraj S Moily, Lakshmi Narayanan Kota, Ram Murthy Anjanappa, Sowmya Venugopal, Radhika Vaidyanathan, Pramod Pal, Meera Purushottam, Sanjeev Jain, and Mahesh Kandasamy. 2014. Trinucleotide repeats and haplotypes at the huntingtin locus in an Indian sample overlaps with European haplogroup a. *PLoS Curr.* 6 (Sept. 2014).

[30] Arjun Narayan, Ariel J. Feldman, Antonis Papadimitriou, and Andreas Haeberlen. 2015. Verifiable Differential Privacy. In *Proceedings of the 10th European Conference on Computer Systems (EuroSys)*. ACM.

[31] Ling Pan and Andrew Feigin. 2021. Huntington’s disease: New frontiers in therapeutics. *Curr. Neurol. Neurosci. Rep.* 21, 3 (Feb. 2021), 10.

[32] H L Paulson and R L Albin. 2011. *Neurobiology of Huntington’s Disease: Applications to Drug Discovery*. CRC Press, Taylor & Francis.

[33] Shizheng Qiu, Jirui Guo, Zhihuai Zhang, Haozheng Liang, Huanyu You, Yang Hu, Guiyou Liu, and Yadong Wang. 2025. MetabolM: a metabolomic language model for multi-disease early prediction and risk stratification. *Nat. Commun.* 16, 1 (Dec. 2025), 11272.

[34] Reda Rawi, Raghvendra Mall, Chen-Hsiang Shen, S Katie Farney, Andrea Shikakolas, Jing Zhou, Halima Bensmail, Tae-Wook Chun, Nicole A Doria-Rose, Rebecca M Lynch, John R Mascola, Peter D Kwong, and Gwo-Yu Chuang. 2019. Accurate prediction for antibody resistance of clinical HIV-1 isolates. *Sci. Rep.* 9, 1 (Oct. 2019), 14696.

[35] Andrea Rizzini, Marco Esposito, Francesco Bruschi, and Donatella Sciuто. 2025. A Private Smart Wallet with Probabilistic Compliance. *arXiv preprint arXiv:2506.04853* (2025).

[36] Robert Anthony Rojas Chávez, Mohammad Fili, Changze Han, Syed A. Rahman, Isaiah G. L. Bicar, Sullivan Gregory, Annika Helverson, Guiping Hu, Benjamin W. Darbro, Jishnu Das, Grant D. Brown, and Hillel Haim. 2024. Mapping the Evolutionary Space of SARS-CoV-2 Variants to Anticipate Emergence of Subvariants Resistant to COVID-19 Therapeutics. *PLOS Computational Biology* 20, 6 (06 2024), 1–33. doi:10.1371/journal.pcbi.1012215

[37] Victoria Sánchez, Mar Masiá, Catalina Robledano, Sergio Padilla, José Manuel Ramos, and Félix Gutiérrez. 2010. Performance of genotypic algorithms for predicting HIV-1 tropism measured against the enhanced-sensitivity Trofile coreceptor tropism assay. *J. Clin. Microbiol.* 48, 11 (Nov. 2010), 4135–4139.

[38] Sacha Servan-Schreiber. 2018. *Cryptographically Certified Hypothesis Testing*. Ph.D. Dissertation. Brown University.

[39] Han-Yi Shih and Wen-Chung Lee. 2017. A five-region hypothesis test for exposure-disease associations. *Sci. Rep.* 7, 1 (July 2017), 5131.

[40] Young Hyun Shin, Chul Min Park, and Cheol Hee Yoon. 2021. An overview of human immunodeficiency virus-1 antiretroviral drugs: General principles and current status. *Infect. Chemother.* 53, 1 (March 2021), 29–45.

[41] Tobin South, Alexander Camuto, and contributors. 2024. ezkl: Zero-Knowledge Machine Learning Inference Framework. <https://github.com/zknduit/ezkl>. Accessed: 2025-02-12.

[42] Sarah J Tabrizi, Michael D Flower, Christopher A Ross, and Edward J Wild. 2020. Huntington disease: new insights into molecular pathogenesis and therapeutic opportunities. *Nat. Rev. Neurol.* 16, 10 (Oct. 2020), 529–546.

[43] Ioanna Tzialla, Abhiram Kothapalli, Bryan Parno, and Srinath Setty. 2021. Transparency Dictionaries with Succinct Proofs of Correct Operation. *IACR Cryptology ePrint Archive* 2021 (2021), 1263. <https://eprint.iacr.org/2021/1263>

[44] Magdalena Väter, Nicolas Rost, Gertrud Eckstein, Susanne Sauer, Alina Tontsch, Angelika Erhardt, Susanne Lucae, Tanja Brückl, Thomas Klopstock, Philipp G Sämann, and Elisabeth B Binder. 2025. Huntington CAG repeat size variations below the Huntington’s disease threshold: associations with depression, anxiety and basal ganglia structure. *Eur. J. Hum. Genet.* 33, 5 (May 2025), 624–632.

[45] Tao Wang, Yasu Ueda, Zhongxing Zhang, Zhiwei Yin, John Matiskella, Bradley C Pearce, Zheng Yang, Ming Zheng, Dawn D Parker, Gregory A Yamanaka, Yi-Fei Gong, Hsu-Tso Ho, Richard J Colombo, David R Langley, Pin-Fang Lin, Nicholas A Meanwell, and John F Kadow. 2018. Discovery of the human immunodeficiency virus type 1 (HIV-1) attachment inhibitor temsavir and its phosphonooxymethyl prodrug fostemsavir. *J. Med. Chem.* 61, 14 (July 2018), 6308–6327.

[46] Andrew Ward, Ashish Sarraju, Sukyung Chung, Jiang Li, Robert Harrington, Paul Heidenreich, Latha Palaniappan, David Scheinker, and Fatima Rodriguez. 2020. Machine learning and atherosclerotic cardiovascular disease risk prediction in a multi-ethnic population. *NPJ Digit. Med.* 3, 1 (Sept. 2020), 125.

[47] Lingwei Xie, Song He, Yuqi Wen, Xiaocheng Bo, and Zhongnan Zhang. 2017. Discovery of novel therapeutic properties of drugs from transcriptional responses based on multi-label classification. *Sci. Rep.* 7, 1 (Aug. 2017), 7136.

[48] Matei Zaharia, Mosharaf Chowdhury, Michael J Franklin, Scott Shenker, and Ion Stoica. 2010. Spark: Cluster computing with working sets. In *2nd USENIX workshop on hot topics in cloud computing (HotCloud 10)*.

[49] Zcash Team. 2023. Halo2: The Halo2 Zero-Knowledge Proving System. <https://zcash.github.io/halo2/concepts/proofs.html>. Accessed: 2026-01-13.

[50] Meng Zhang, Yongqi Zheng, Xiagela Maidaiti, Baosheng Liang, Yongyue Wei, and Feng Sun. 2024. Integrating Machine Learning into Statistical Methods in Disease Risk Prediction Modeling: A Systematic Review. *Health Data Science* 4 (2024), 0165. doi:10.34133/lds.0165 arXiv:<https://spj.science.org/doi/pdf/10.34133/lds.0165>

[51] Yizheng Zhu, Yuncheng Wu, Zhaojing Luo, Beng Chin Ooi, and Xiaokui Xiao. 2024. Secure and Verifiable Data Collaboration with Low-Cost Zero-Knowledge Proofs. *Proceedings of the VLDB Endowment* 17, 9 (2024), 2321–2334. doi:10.14778/3665844.3665860

[52] Boitumelo J L Zuze, Botshelo T Radibe, Wonderful T Choga, Ontlametse T Bareng, Natasha O Moraka, Dorcas Maruapula, Kedumetse Seru, Patrick Mokgethi, Baitshepi Mokaleng, Nokuthula Ndlovu, Nametsa Kelentse, Molly Pretorius-Holme, Roger Shapiro, Shahin Lockman, Joseph Makhema, Vlad Novitsky, Kaelo K Seata, Sikhulile Moyo, and Simani Gaseitsiwe. 2023. Fostemsavir resistance-associated polymorphisms in HIV-1 subtype C in a large cohort of treatment-naïve and treatment-experienced individuals in Botswana. *Microbiol. Spectr.* 11, 6 (Dec. 2023), e0125123.

A Ethics Consideration

There are no ethical issues with the data. No real human data were used in this study. The distribution of CAG repeats in four population studies were averaged and used to generate a single distribution for each of the groups (healthy and diseased). The Huntington’s dataset were then generated from these distributions. The Temsavir resistance data describe virus sequences (amino acids at four positions of the Env protein) and the measured resistance of the corresponding viruses to Temsavir. No human sequence data were available to the authors. No data were available to the authors that could identify the people from whom the viruses were isolated.

B Open Science

B.1 Artifact Inventory

The following artifacts are required to evaluate the core contributions of CoSMETIC : A Python 3.11 reference implementation of CoSMETIC , including: (i) leaf-level transformations and aggregation logic, (ii) Sparse Merkle Tree (SMT/CSMT) construction using Poseidon hashing, (iii) proof generation and verification logic using EZKL (Halo2 backend), and (iv) experiment drivers for the evaluated statistical workflows.

Scripts for reproducing the paper’s results for: (i) Kolmogorov–Smirnov (KS), (ii) Logistic Likelihood-Ratio Test (LRT), and (iii) Logistic Accuracy (ACC), including configuration of fixed-point precision (ZKP_SCALER) and SMT height (TREE_HEIGHT).

Documentation describing: (i) environment setup (Python dependencies and/or Docker), (ii) required runtime environment variables, (iii) commands to run the drivers and/or invoke the prover APIs, and (iv) expected outputs (proof files and downloadable artifacts such as verification keys and settings).

A Docker Compose stack providing three Flask APIs for proof generation and verification such as api_acc.py (ACC), api_ks.py (KS), and api_lrt.py (LRT), and a statistics logger for CPU, memory, container metrics. The repository also includes a Makefile to build images locally.

B.2 Anonymous Artifact Access During Review

To preserve double-blind review, all artifacts are hosted in an anonymous repository that is accessible to the program committee:

<https://anonymous.4open.science/r/cosmetic-D845/>

The repository contains the full implementation, scripts, and documentation needed to run the system and reproduce results. Reviewers can reproduce all experiments by running the complete prover

stack using the provided `docker-compose.yml`, which builds the Sparse Merkle Trees, compiles EZKL circuits, and exposes the ACC, KS, and LRT prover APIs for proof generation, verification, and artifact download.

B.3 Reproduction Pathways

We support reproduction of all experiments by running the prover API stack using containers via the provided `docker-compose.yml`. The stack builds the Sparse Merkle Trees, compiles EZKL circuits, and exposes three prover APIs: ACC on port 5012, KS on port 5013, and LRT on port 5014. The APIs support job-based proof generation, verification, and download of proof bundles and circuit artifacts, including compiled circuits, verification keys, and settings.

B.4 Unavailable or Restricted Artifacts

This work does not require sharing private clinical/genomic records. The evaluated case studies are used to motivate the statistical workflows, while the artifact provides the full implementation and the code paths needed to reproduce the reported measurements and figures.

Some environments may encounter Docker Hub unauthenticated pull-rate limits when using the prebuilt images referenced by the Compose stack. This does not restrict access to the artifacts: reviewers can (i) authenticate to Docker Hub if desired, or (ii) build images locally using the provided `Makefile`. No artifacts are withheld due to licensing, privacy, or responsible disclosure constraints.

C Proofs

C.1 Proof of Proposition 1

Case 1.1 (Inclusion implies Membership): For this case it is sufficient to prove that $(u \in U) \implies \mathcal{M}([u, \delta] | R) = 1$. If we consider $u \in U$, Properties 1 and 4 imply the existence of unique user and transform salts given by μ, τ respectively. Leveraging Properties 4 and 5, we know that the data tuple (δ, μ, τ) for user $u \in U$ corresponds to a unique leaf index given by \mathcal{N}_u such that the binary representation of \mathcal{N}_u is equal to $\text{hash}(\mathcal{L}^s(\delta, \mu, \tau))$. Given the collision resistance property of hash , uniqueness of μ and τ , we can state that $\mathcal{L}(\delta) \in \Delta_U^L$ which corresponds to $\mathcal{M}([u, \delta] | R) = 1$

Case 1.2 (Exclusion implies Non Membership): For this case, it is sufficient to prove that $(u \notin U) \implies \mathcal{M}([u, \delta] | R) = 0$. If $u \notin U$, then $\mathcal{L}(\delta) \notin \Delta_U^L$ which would mean that $\mathcal{M}([u, \delta] | R) = 0$ according to Definition 1.

Case 2.1 (Membership implies Inclusion): For this case, it is sufficient to show that $\mathcal{M}([u, \delta] | R) = 1 \implies (u \in U)$. We know using Definition 1 that $\mathcal{M}([u, \delta] | R) = 1$, can only occur when $\exists \mathcal{L}(\delta) \in \Delta_U^L$. As a result, we can find unique user and transform salt vectors $\mu \in \mathbb{R}^{s_u}$ and $\tau \in \mathbb{R}^{s_t}$ to obtain an augmented data tuple (δ, μ, τ) such that $H = \text{hash}(\mathcal{L}^s(\delta, \mu, \tau))$. Using Properties 4 and 5, we can state that $\exists \mathcal{N} = \text{Decimal}(H)$ and $\varphi_N^0 \neq \mathcal{L}^s(\emptyset)$ thereby demonstrating inclusion $u \in U$.

Case 2.2 (Non Membership implies Exclusion): For this case, it is sufficient to demonstrate that $\mathcal{M}([u, \delta] | R) = 0 \implies (u \notin U)$. We know that $\mathcal{M}([u, \delta] | R) = 0$ occurs only when $\mathcal{L}(\delta) \notin \Delta_U^L$. Assuming sufficient entropy in the salt strings and given collision resistance, we can say that for all combinations of $\hat{\mu} \in \mathbb{R}^{s_u}, \hat{\tau} \in \mathbb{R}^{s_t}$

the following relation holds where $H_u = \text{hash}(\mathcal{L}^s(\delta_u, \mu_u, \tau_u))$

$$\Pr \left[\text{hash}(\mathcal{L}^s(\delta, \hat{\mu}, \hat{\tau})) = H_u \right] \leq \text{negl}(K) \quad \forall u \in U \quad (17)$$

Therefore, it is not possible to find some $\hat{\mu}, \hat{\tau}$ for which $\varphi_N^0 \neq \mathcal{L}^s(\emptyset)$ where $\mathcal{N} = \text{Decimal}(\text{hash}(\mathcal{L}^s(\delta, \hat{\mu}, \hat{\tau})))$

C.2 Proof of Proposition 2

PROOF. We will present two cases for completing the proof.

$$\text{Case 1: } (\Phi_{\mathcal{L}^s}^u = 1 \text{ and } \Phi_{\mathcal{A}^l}^{u,k} = 1 \implies \mathcal{M}([u, \delta] | \mathcal{R}(\mathcal{A}, \mathcal{L}, U))) \quad (18)$$

For this case, we know that leaf and aggregation proof artifacts are verifiable.

Case 1.1: Let us assume that there exists a user $u \in U$ with datum δ such that

$$\Phi_{\mathcal{L}^s}^u = 1 \text{ and } \Phi_{\mathcal{A}^l}^{u,k} = 1 \quad (18)$$

$$\mathcal{M}([u, \delta] | \mathcal{R}(\mathcal{A}, \mathcal{L}, U)) = 0 \quad (19)$$

If $\Phi_{\mathcal{L}^s}^u = 1$ and $\Phi_{\mathcal{A}^l}^{u,k} = 1$, then it also implies that there exists some user u such that Definition 5 applies.

Using Proposition 1, we already know that when $u \in U$ and $\mathcal{M}([u, \delta] | \mathcal{R}(\mathcal{A}, \mathcal{L}, U)) = 1$. This leads to a contradiction of our earlier stated assumption.

Case 1.2: Let us assume that there exists a user $u \notin U$ with datum δ such that

$$\Phi_{\mathcal{L}^s}^u = 1 \text{ and } \Phi_{\mathcal{A}^l}^{u,k} = 1 \quad (20)$$

$$\mathcal{M}([u, \delta] | \mathcal{R}(\mathcal{A}, \mathcal{L}, U)) = 1 \quad (21)$$

Using a similar logic as above, we argue that using Proposition 1, $\mathcal{M}([u, \delta] | \mathcal{R}(\mathcal{A}, \mathcal{L}, U)) = 0$ when $u \notin U$ leading us to a contradiction of $\mathcal{M}([u, \delta] | \mathcal{R}(\mathcal{A}, \mathcal{L}, U)) = 1$

Using both Case 1.1 and Case 1.2, we can clearly state that a user who satisfies $\Phi_{\mathcal{L}^s}^u = 1$ and $\Phi_{\mathcal{A}^l}^{u,k} = 1$ also necessarily leads to the correct output of the membership function $\mathcal{M}([u, \delta] | \mathcal{R}(\mathcal{A}, \mathcal{L}, U))$.

$$\text{Case 2 } (\mathcal{M}([u, \delta] | \mathcal{R}(\mathcal{A}, \mathcal{L}, U)) \implies \Phi_{\mathcal{L}^s}^u = 1 \text{ and } \Phi_{\mathcal{A}^l}^{u,k} = 1) \quad (22)$$

To prove sufficiency, let us consider two sub cases.

Case 2.1: Assume we have a user $u \in U$ with datum δ such that $\mathcal{M}([u, \delta] | \mathcal{R}(\mathcal{A}, \mathcal{L}, U)) = 1$. Let us assume either $\Phi_{\mathcal{L}^s}^u = 0$ or $\Phi_{\mathcal{A}^l}^{u,k} = 0$ for some k . We know that if $\Phi_{\mathcal{L}^s}^u = 0$, then

$$\mathcal{L}^s([\delta, \mu, \tau]; \theta_{\mathcal{L}^s}) \neq [\hat{\mathcal{L}}(\delta, \mu; \theta_{\hat{\mathcal{L}}}), \tau], \quad \tau \in \mathbb{R}^{s_t} \quad (22)$$

which is a contradiction of Property 2 if $u \in U$. Therefore $\Phi_{\mathcal{L}^s}^u = 1$.

Similarly, we know that if $\Phi_{\mathcal{A}^l}^{u,k} = 0$ for some k $u \in U$ then this is a violation of Property 3 which implies an inconsistent Merkle path. Further using Property 6 we can also assert that given user $u \in U$ corresponds to a consistent Merkle path. This implies a contradiction establishing the fact that if $u \in U$ it necessarily implies that $\Phi_{\mathcal{L}^s}^u = 1$ and $\Phi_{\mathcal{A}^l}^{u,k} = 1$.

Case 2.2 Assume we user $u \notin U$, with $\mathcal{M}([u, \delta] | \mathcal{R}(\mathcal{A}, \mathcal{L}, U)) = 0$. As before, we suppose that either $\Phi_{\mathcal{L}^s}^u = 0$ or $\Phi_{\mathcal{A}^l}^{u,k} = 0$ for some k . Since $u \notin U$, this implies that $\mathcal{L}^s([\delta, \mu, \tau]; \theta_{\mathcal{L}^s}) = \mathcal{L}^s(\emptyset)$. However, we also know that if $\Phi_{\mathcal{L}^s}^u = 0$, then

$$\mathcal{L}^s([\delta, \mu, \tau]; \theta_{\mathcal{L}^s}) \neq [\hat{\mathcal{L}}(\delta, \mu; \theta_{\hat{\mathcal{L}}}), \tau], \quad \tau \in \mathbb{R}^{s_t} \quad (23)$$

This implies that we encounter a contradiction

$$\mathcal{L}^s([\delta, \mu, \tau]; \theta_{\mathcal{L}^s}) \neq \mathcal{L}^s(\emptyset) \implies u \in U \quad (24)$$

Similarly, we know that if $\Phi_{\mathcal{A}^l}^{u,k} = 0$ for some $k \in U$ then this is a violation of Property 3 which implies an inconsistent Merkle path. As before, using Property 6 we can also assert that even when user $u \notin U$ corresponds to a consistent Merkle path. This implies a contradiction establishing the fact that if $u \notin U$ it necessarily implies that $\Phi_{\mathcal{L}^s}^u = 1$ and $\Phi_{\mathcal{A}^l}^{u,k} = 1$. \square

C.3 Proof of Proposition 3

PROOF. We already know under Proposition 2 that verifying the LTR and MRP proofs is a necessary and sufficient condition for realizing the membership of user u in a reduction operation given $R(\mathcal{A}, \mathcal{L}, U^{inc})$.

Let Ω_δ^u denote the raw user data record δ^u of user u as contained in witness $\Omega_{LTR}^u \in \Omega^u$. We assume a compromised CRO possessing an extractor \mathcal{E}^C that produces a valid proof $\hat{\Pi}^u$ with an incorrect witness $\hat{\Omega}^u = \mathcal{E}^C(\Omega^u)$ such that

$$\hat{\Phi}^{(\delta, \mu)} = \text{VerInc}(H^{(\delta, \mu)}, H^{leaf}, \hat{\Pi}^u, H^{root}, H^\eta, vk_{\mathcal{L}^s}, vk_{\mathcal{A}^l}) = 1 \quad (25)$$

There are two possible outcomes to generate an incorrect witness $\hat{\Omega}^u$

Case 1 (Incorrect salted raw data): In this case, we consider a scenario wherein a compromised the CRO tries to generate a valid zk-SNARK $\hat{\Pi}^u$ that maintains the consistency between the first input in $\hat{\Pi}^u$ and the salted raw user data hash $H^{(\delta, \mu)}$.

More technically, CRO tries to generate a valid $\hat{\Pi}_{\mathcal{L}^s}^u$ using an incorrect witness $\hat{\Omega}^u = \{\hat{\Omega}_{LTR}^u, \Omega_{MRP}^u\}$. To prove using contradiction, we assume there exists a perturbed salted raw data tuple $\hat{\Omega}_{LTR}^u = \{\hat{\delta}_u, \hat{\mu}_u, \tau_u\}$ that leads to $\hat{\Phi}^{(\delta, \mu)} = 1$. We denote the LTR constraint set \mathcal{Z}_{LTR}^u for user u as defined by Equations (26)-(27).

$$\hat{\Pi}_{\mathcal{L}^s}^u[\text{Input1}] = H^{(\delta, \mu)} \quad (26)$$

$$\hat{\Pi}_{\mathcal{L}^s}^u[\text{Input2}] = H^\tau \quad (27)$$

$$\hat{\Pi}_{\mathcal{L}^s}^u[\text{Output}] = H_u^{leaf} \quad (28)$$

We know from Algorithm 9 that $(H^{(\delta, \mu)}, H^\tau, H_u^{leaf}) \in \mathcal{Z}_{LTR}^u$ must hold for LTRVerify to return a success as given in Equation (29).

$$\text{LTRVerify}(vk_{\mathcal{L}^s}, \Pi_{\mathcal{L}^s}^u, H^{(\delta, \mu)}, H_u^{leaf}) = 1 \quad (29)$$

We also know from the knowledge-soundness property of Halo2 [49], that

$$\Pr[\text{Verify}(vk_{\mathcal{L}^s}, \hat{\Pi}_{\mathcal{L}^s}^u) = 1 \wedge (H^{(\delta, \mu)}, H^\tau, H_u^{leaf} \in \mathcal{Z}_{LTR}^u)] \leq \text{negl}(\lambda)$$

This leads us to a contradiction thereby establishing the fact that a compromised CRO cannot generate a valid zk-SNARK that proves the inclusion of the incorrect data for any user.

Case 2 (Incorrect MRP proof): We consider a scenario where a compromised CRO generates a valid proof $\hat{\Pi}_{\mathcal{A}^l}^u$ using an incorrect MRP witness $\hat{\Omega}_{MRP}^u$. Using contradiction, we assume that there exists a valid zk-SNARK $\hat{\Pi}_{\mathcal{A}^l}^{u,k} \in \mathcal{Z}_{\mathcal{A}^l}^u$ that is generated using an incorrect $\hat{\Omega}_{MRP}^u$.

Case 2.1 (Incorrect Selector Bit Path): In this case, to prove using contradiction, we assume that the CRO supplies $\hat{\Pi}_{\mathcal{A}^l}^u$ that corresponds to an incorrect salted leaf transform \hat{H}_u^{leaf} instead of the

genuine H_u^{leaf} for user u . However, we know that \hat{H}_u^{leaf} cannot lead to a successful evaluation of LTRVerify at the verifier level due to the knowledge-soundness argument of Case 1. As a consequence, by contradiction we can say that the CRO cannot use an incorrect selector bit path sequence \hat{B} instead of the correct selector bit path B without violating the knowledge-soundness property.

Case 2.2 (Incorrect MRP hop inputs): We assume that the CRO uses an incorrect hop witness for some level $1 \leq k \leq K$ while using the correct selector bit path index B . For a particular level k , we denote MRP constraint set as $\mathcal{Z}_{MRP}^{k,u}$ which is defined by Equations (30)-(34).

$$\text{hash}(B[k]) = H^{k,b} \text{ and } \text{Bin}(H_u^{leaf}) = B \quad (30)$$

$$H^{k,L} = \begin{cases} \hat{\Pi}_{\mathcal{A}^l}^{k-1}[\text{Parent}], & \text{if } B[k] = 0 \\ \hat{\Pi}_{\mathcal{A}^l}^k[\text{LeftInput}], & \text{otherwise} \end{cases} \quad (31)$$

$$H^{k,R} = \begin{cases} \hat{\Pi}_{\mathcal{A}^l}^k[\text{RightInput}], & \text{if } B[k] = 0 \\ \hat{\Pi}_{\mathcal{A}^l}^{k-1}[\text{Parent}] & \text{otherwise} \end{cases} \quad (32)$$

$$\hat{\Pi}_{\mathcal{A}^l}[\text{Bit}] = H^{k,b} \quad (33)$$

$$\hat{\Pi}_{\mathcal{A}^l}[\text{Nonce}] = H^\eta \quad (34)$$

We know from Algorithm 10 that for a particular level k Equation (35) must be fulfilled to successfully validate MRP hop proof artifact.

$$\text{MRPHopVerify}(vk_{\mathcal{A}^l}, \hat{\Pi}_{\mathcal{A}^l}^k, H^{k,L}, H^{k,R}, H^{k,b}, H^\eta) = 1 \quad (35)$$

By applying the knowledge-soundness argument we know that the following condition holds.

$$\Pr[\text{Verify}(vk_{\mathcal{A}^l}, \hat{\Pi}_{\mathcal{A}^l}^u) = 1 \wedge (H^{k,L}, H^{k,R}, H^{k,b}, H^\eta) \in \mathcal{Z}_{MRP}^{k,u}] \leq \text{negl}(\lambda)$$

This is a direct contradiction of our assumption which completes the proof. \square

C.4 Proof of Proposition 4

PROOF. Consider a subset $\mathcal{D}_q \subseteq \Delta_U^{\mathcal{L}^s}$ of q ordered leaf nodes, where $\mathcal{D}_q = \{\varphi_1^{0,s}, \varphi_2^{0,s} \dots \varphi_q^{0,s}\}$ and $q \leq 2^K$. Further consider the lower and upper bound decimal representation limits of the hash of the individual leaves of set \mathcal{D}_q defined in Equations (36) and (37).

$$L^q = \min(\{\text{Decimal}[\text{hash}(\varphi_1^{0,s})], \dots, \text{Decimal}[\text{hash}(\varphi_q^{0,s})]\}) \quad (36)$$

$$U^q = \max(\{\text{Decimal}[\text{hash}(\varphi_1^{0,s})], \dots, \text{Decimal}[\text{hash}(\varphi_q^{0,s})]\}) \quad (37)$$

Let $H_{\mathcal{D}_s}^{root}$ be the subtree root corresponding to the ordered transformed leaf set \mathcal{D}_q . Now consider a $\hat{\phi}$, such that we obtain another ordered set $\hat{\mathcal{D}}_q = \mathcal{D}_s \cup_{ord} \{\hat{\phi}\}$ with $H_{\mathcal{D}_s}^{root}$ as the subtree root of $\hat{\mathcal{D}}_q$.

To prove by contradiction, let us assume that $H_{\hat{\mathcal{D}}_q}^{root} = H_{\mathcal{D}_q}^{root}$. We know that we can define $\hat{H} = \text{hash}(\hat{\phi})$ for which

$$L^q \leq \text{Decimal}[\hat{H}] \leq U^q, \text{ and } H_{\hat{\mathcal{D}}_q}^{root} = H_{\mathcal{D}_q}^{root} \quad (38)$$

However, using Property 2, we know that all leaf transformations in $\hat{\mathcal{D}}_q$ must be unique. Therefore, using the computational

aggregation primitive $\mathcal{A}^s(\cdot; \theta_{\mathcal{A}^s})$ as defined in Equation (14) we obtain Equation (39).

$$\mathcal{A}^s(\mathcal{D}_q; \theta_{\mathcal{A}^s}) \neq \mathcal{A}^s(\hat{\mathcal{D}}_{\mathcal{U}}; \theta_{\mathcal{A}^s}) \quad (39)$$

As a consequence of Equation (39) along with the properties of the hash function defined in Definition 5, we can say that $H_{\mathcal{D}_q}^{\text{root}} \neq H_{\hat{\mathcal{D}}_q}^{\text{root}}$. As a result, we violate Definition 4 which governs the construction of the CSMT, thereby completing the proof. \square

C.5 Algorithm for detecting data exclusivity

Algorithm 8 defines function `VerifyDataExclusivity` that consumes a reference to the Merkle root of the PHR database \mathcal{P} , the set of non default salted leaf nodes \mathcal{T} . Additionally, the function also ingests the hash tuple of raw data, user salt $H^{(\delta_u, \mu_u)}$ and transform salt H^{τ_u} for each user u included in the clinical study. The set of all such hash tuples is denoted by \mathcal{H} . As part of Assumption 1, we know that each hash tuple $(H^{(\delta_u, \mu_u)}, H^{\tau_u}) \in \mathcal{H}$ included in the clinical study must also be substantiated by a simple corresponding Merkle proof from the PHR database. Collectively, the sets \mathcal{H} and \mathcal{P} can be pre-committed by the CRO as a precursor to Algorithm 2. As a result, in Algorithm 8, we check for the PHR Merkle consistency $(H^{(\delta_u, \mu_u)}, H^{\tau_u}) \in \mathcal{P}$ while ensuring that each user hash tuple is also included in \mathcal{H} . Next, we analyze each LTR proof and generate a set of non-default leaf node hashes that serve as a foundation for MRP driven exclusivity checks.

We carry out a tree traversal in a depth-first manner to create a set of nodes that have been encountered as a consequence of non-default leaves in the CSMT. To ensure data exclusivity as defined in Definition 8 and as guaranteed by Proposition 4, we check two criteria. First, the set of leaf nodes encountered in MRP tree traversal must be the same as the ones found by analyzing the LTR proofs of all included users. Second, there each non-leaf MRP node must have at least one-leaf ancestor. Given successful evaluation of both criteria, we can guarantee data exclusivity.

D Supplementary Text

D.1 Case Studies

D.1.1 Huntington Disease Huntington's disease (HD) is a hereditary neurodegenerative disorder caused by changes in the HTT gene located on chromosome 4 [14, 31]. The disease affects the brain and manifests with motor abnormalities, cognitive decline, and behavioral symptoms [32, 42]. The genomic changes that cause the disease consist of an abnormal expansion of the three-nucleotide sequence Cytosine–Adenine–Guanine (CAG) in the segment of the gene that encodes for the Huntingtin protein [24]. The CAG trinucleotide sequence encodes for the amino acid glutamine, resulting in an elongated polyglutamine stretch in the protein. This aberrant form is prone to aggregation, leading to progressive loss of neuronal function and death of these cells, mainly in the striatum and cortex regions of the brain. The number of CAG repeats correlates strongly with the likelihood for symptoms, disease onset, and severity [20]. In healthy individuals, the average CAG repeat number is 17, while in HD patients it is approximately 40 [10, 16, 29, 44].

As genomic testing is increasingly used in clinical practice, the need to maintain privacy of these data has also gained attention.

Algorithm 8 Data Exclusivity Check

```

1: function VERIFYDATAEXCLUSIVITY( $\mathcal{H}^{\text{inc}}, \mathcal{P}, \mathcal{T}, \Pi_{\text{CSMT}}^{\text{U}^{\text{inc}}}$ )
   ▷ initialize encountered leaf nodes and raw data records
2:   NodesLTR  $\leftarrow \emptyset$ 
3:   for  $\Pi_{\mathcal{L}_s}^u \in \Pi_{\text{CSMT}}^{\text{U}^{\text{inc}}}$  do
4:     retrieve LTR proof  $\Pi_{\mathcal{L}_s}^u$  from  $\Pi_{\text{CSMT}}^{\text{U}^{\text{inc}}}$  for level  $k$ 
5:     retrieve  $H_u^{\text{leaf}}$  and  $H^{(\delta_u, \mu_u)}$  and  $H^{\tau_u}$  from  $\Pi_{\mathcal{L}_s}^u$ .
6:     if  $(H^{(\delta_u, \mu_u)}, H^{\tau_u}) \in \mathcal{P}$  and  $(H^{(\delta_u, \mu_u)}, H^{\tau_u}) \in \mathcal{H}$  then
7:       NodesLTR  $\leftarrow$  NodesLTR  $\cup \{H_u^{\text{leaf}}\}$ 
8:     end if
9:   end for
   ▷ initialize encountered nodes and their subtree leaves
10:  NodesMRP  $\leftarrow \emptyset$ 
11:  for  $H^{\text{leaf}} \in \{\mathcal{T} : \text{SaltedLeafSet}\}$  do
12:    obtain MRP proof set  $\Pi_{\text{CSMT}}^{\text{leaf}} \leftarrow \Pi_{\text{CSMT}}^{\mathcal{T}}$  for leaf
13:    for  $k = 1$  to  $K$  do
14:      retrieve MRP proof  $\Pi_{\mathcal{A}^l}^k \leftarrow \Pi_{\mathcal{A}^l}^u [k]$  for level  $k$ 
15:      retrieve sibling hash  $v_{\text{sib}}$  from  $\Pi_{\mathcal{A}^l}^k$ 
16:      retrieve parent hash  $v$  from  $\Pi_{\mathcal{A}^l}^k$ 
17:      if  $v_{\text{sib}} \notin \text{Nodes}$  then
18:        NodesMRP[ $v_{\text{sib}}$ ].Leaves  $\leftarrow \emptyset$ 
19:      end if
20:      if  $v \notin \text{Nodes}$  then
21:        NodesMRP[ $v$ ].Leaves  $\leftarrow \{H^{\text{leaf}}\}$ 
22:      else
23:        NodesMRP[ $v$ ].Leaves  $\leftarrow \text{Nodes}[v].\text{Leaves} \cup \{H^{\text{leaf}}\}$ 
24:      end if
25:    end for
26:  end for
   ▷ each leaf must result from a raw data record
27:  if  $\bigcup_{\forall v} (\text{NodesMRP}[v].\text{Leaves}) \neq \text{NodesLTR}$  then
28:    return spurious leaf existence detected
29:  end if
   ▷ each MRP node must have at least one leaf descendant
30:  for  $v \in \text{NodesMRP}$  do
31:    if  $\text{NodesMRP}[v].\text{Leaves} = \emptyset$  and  $v \notin \mathcal{T}$  then
32:      return spurious leaf existence detected
33:    end if
34:  end for
35: end function

```

Hypothesis testing to address genomic research questions is critical for our ability to decipher the propensity of people to develop diseases and for their prevention. However, such tests require access to the data, and sharing of personal genomic information raises serious privacy concerns. For example, leakage of the CAG repeat number of an individual can have significant implications for the individual and their families. Thus, analysis of the data should be performed privately, while maintaining the ability to provide regulatory entities the assurance that all tests were performed correctly.

The fundamental basis for hypothesis testing is that the correct data are used for computing the test statistic. For clinical studies, the equivalent assumption is that all intended study participants were indeed included in the analysis, and that non-participants were not

included. Thus, for analyses conducted privately, the study managers must provide verifiable proof that the intended participants' data were included in computing the test statistic and that no data from non-participants were used. Here we present the case study for the distribution of CAG repeats between healthy individuals and people with symptoms of HD. To this end, we used two datasets that capture the distribution of CAG repeats in healthy individuals and in those presenting with the clinical HD syndrome. The values are based on data reported in four studies that sequenced people across different ancestries and classified them according to the clinical findings [10, 16, 29, 44]. Two independent sample sets were constructed, each comprising 50 individuals, which correspond to the healthy and HD groups. To evaluate the hypothesis that the distributions of CAG repeat lengths differ significantly between people with HD symptoms and healthy people, we used a two-sample Kolmogorov-Smirnov (KS) test. The proposed privacy-preserving methodology supports both proof of membership (i.e., verifying that data from true participants were included in the computation) and proof of non-membership (i.e., ensuring that data from other individuals were not used). Importantly, these assurances and the final test statistic value are obtained without disclosing any clinical data or the CAG repeat number of the participants.

D.1.2 HIV-1 Antiviral therapeutics are used to reduce viral loads in individuals infected by human immunodeficiency virus type 1 (HIV-1). Different classes of antiviral agents target distinct HIV-1 proteins, including reverse transcriptase, protease, integrase and the envelope glycoproteins (Env) [40]. Due to mutations in the genes that encode these proteins, some infected individuals harbor viruses that are resistant to the effects of the inhibitors [27]. Pre-existing resistant viruses result in partial or complete lack of a clinical response to the treatment. To prevent such outcomes, and select the most appropriate therapeutic, there is a need to determine before treatment the resistance profile of the viruses that infect each person.

One screening approach is based on direct phenotyping, by amplifying the virus genes from clinical samples and then testing the proteins they produce in vitro to determine their resistance to each therapeutic. The PhenoSense commercial test is most commonly used for this purpose and provides actionable information for clinical decision making [12]. However, this approach is time consuming (usually one month or longer) and costly. An alternative strategy developed in recent years involves sequencing of the viruses in patient samples, and use of the sequence data to infer resistance to each therapeutic. The approach is rapid and inexpensive. However, some HIV-1 proteins, and particularly the Env, are complex and exhibit high diversity. As a result, inferences of phenotype based on sequence are not trivial [34, 37].

Similar to human genomic data, sequence and phenotypic data of viruses collected for clinical purposes are maintained private at the clinical research organizations where they are analyzed. While such data can be applied locally to test and optimize machine learning algorithms to predict resistance by sequence, the relative performance of the models and the inclusion of specific samples in their development cannot be proven due to inability to share the raw data.

In this case study, we examined the Env-targeting therapeutic BMS-626529 (Temsavir, TMR) [26, 45]. TMR is approved by the US Food and Drug Administration (FDA) and effectively reduces viral loads in HIV-infected individuals [1, 18]. We have recently shown that the sensitivity of HIV-1 to TMR can be estimated well by amino acid sequence. Mutations at positions 375, 426, 434 and 475 of the Env protein account for most of the resistance to TMR observed in treated patients [11, 52]. Here we used a dataset composed of 564 samples from distinct HIV-infected individuals. Each sample was associated with four features that describe the amino acid sequence at the above Env positions, and a resistance value measured in vitro using the PhenoSense GT assay.

E Supplementary Algorithms

E.1 Verifying zk-SNARK Artifacts

Algorithm 9 defines function `LTRVerify` as a means to verify LTR proofs based on verification key $vk_{\mathcal{L}^s}$, LTR zk-SNARK $\Pi_{\mathcal{L}^s}$, hash of raw salted user data, transform salt and salted leaf transform $H^{raw}, H^{\tau}, H^{leaf}$ respectively. The `LTRVerify` function primarily validates the given zk-SNARK using the verification key using the `Verify` function. Additionally, it ensures hash consistency between supplied hashes $H^{raw}, H^{\tau}, H^{leaf}$ and the input and output hashes contained in the provided zk-SNARK. The final verification output of the function depends on successfully passing the criteria for zk-SNARK validation as well as the hash consistency check.

Algorithm 9 Verifying LTR Proof

```

1: function LTRVERIFY( $vk_{\mathcal{L}^s}, \Pi_{\mathcal{L}^s}, H^{raw}, H^{\tau}, H^{leaf}$ )
2:    $\Phi_{us} \leftarrow 0, \Phi_{ts} \leftarrow 0, \Phi_{output} \leftarrow 0$  and  $\Phi_{zk} \leftarrow 0$ 
    $\triangleright$  initialize input, output and LTR verification statuses
3:    $\Phi_{zk} \leftarrow \text{Verify}(vk_{\mathcal{L}^s}, \Pi_{\mathcal{L}^s})$ 
4:   if  $\Pi_{\mathcal{L}^s}[\text{Input1}] = H^{raw}$  then  $\triangleright$  user data consistency
5:      $\Phi_{us} \leftarrow 1$ 
6:   end if
7:   if  $\Pi_{\mathcal{L}^s}[\text{Input2}] = H^{\tau}$  then  $\triangleright$  transform salt consistency
8:      $\Phi_{ts} \leftarrow 1$ 
9:   end if
10:  if  $\Pi_{\mathcal{L}^s}[\text{Output}] = H^{leaf}$  then  $\triangleright$  output consistency
11:     $\Phi_{output} \leftarrow 1$ 
12:  end if
13:  return  $\Phi_{zk} \cap \Phi_{input} \cap \Phi_{output}$ 
14: end function

```

In Algorithm 10 we present function `MRPHopVerify` which handles the verification of per-hop MRP proofs. The `MRPHopVerify` function consumes the verification key for aggregator circuit, zk-SNARK proof artifact as well as the hashes of the left and right sibling, selector bit path index array and the nonce. These input variables are denoted by $vk_{\mathcal{A}l}, \Pi_{\mathcal{A}l}, H^L, H^R, H^b, H^{\eta}$ respectively. The function validates the provided zk-SNARK using the verification key and checks for hash consistency of left and right siblings, selector bits and the nonce. Passing each criteria results in an overall success of the `MRPHopVerify` function.

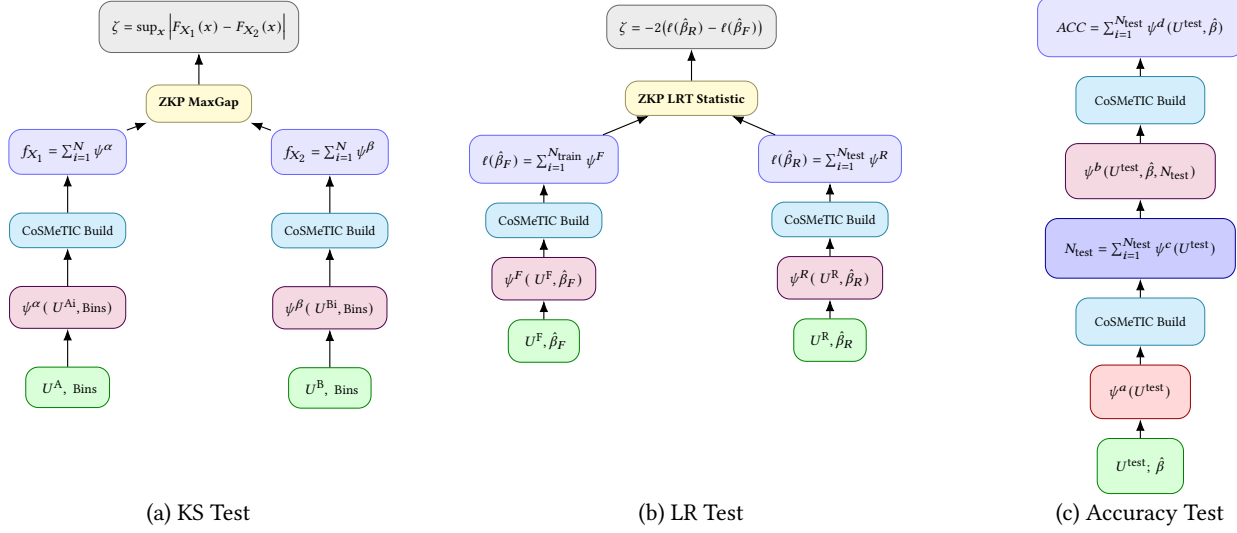


Figure 4: CoSMETIC workflows for KS, LRT, and accuracy.

Algorithm 10 Verifying MRP Hop Proofs

```

1: function MRPHopVERIFY( $vk_{\mathcal{A}^l}, \Pi_{\mathcal{A}^l}, H^L, H^R, H^b, H^\eta$ )
   ▷ initialize MRP verification statuses
2:    $\Phi_L \leftarrow 0, \Phi_R \leftarrow 0, \Phi_b \leftarrow 0, \Phi_{output} \leftarrow 0$  and  $\Phi_{zk} \leftarrow 0$ 
3:
   ▷ MRP SNARK verification
4:    $\Phi_{zk} \leftarrow \text{Verify}(vk_{\mathcal{A}^s}, \Pi_{\mathcal{A}^s})$ 
5:   if  $\Pi_{\mathcal{A}^s}[\text{LeftInput}] = H^L$  then      ▷ left input consistency
6:      $\Phi_L \leftarrow 1$ 
7:   end if
8:   if  $\Pi_{\mathcal{A}^s}[\text{RightInput}] = H^R$  then      ▷ right input consistency
9:      $\Phi_R \leftarrow 1$ 
10:  end if
11:  if  $\Pi_{\mathcal{A}^s}[\text{Bit}] = H^b$  then      ▷ selector bit consistency
12:     $\Phi_b \leftarrow 1$ 
13:  end if
14:  if  $\Pi_{\mathcal{A}^s}[\text{Nonce}] = H^\eta$  then      ▷ nonce consistency
15:     $\Phi_\eta \leftarrow 1$ 
16:  end if
17:  return  $\Phi_{zk} \cap \Phi_L \cap \Phi_R \cap \Phi_b \cap \Phi_\eta$ 
18: end function

```

E.2 Kolmogorov-Smirnov (KS) Test

We first consider the two-sample Kolmogorov-Smirnov (KS) test, which compares the empirical distributions of Group A (healthy) and Group B (HD). The computations steps are outlined in Algorithm 11. We begin by defining the transformation and aggregation circuits. The key leaf-level transformation is the bin-count operation, denoted by \mathcal{L}_{BC}^s , which determines the bin assignment of each data point given a pre-specified bin vector $\theta_{\mathcal{L}_{BC}^s}$. The output of this transformation is a vector of the same length as the bin vector, with all entries equal to zero except for the position corresponding to the bin into which the data point falls. The aggregation function, \mathcal{A}_{sum}^l , computes the element-wise vector sum

across observations. In the CoSMETIC pipeline, each group is evaluated independently, followed by a zero-knowledge computation that evaluates the maximum absolute difference (see Algorithm 13) between their cumulative distributions. We show the verification process for KS test in Algorithm 12.

Algorithm 11 Two-sample KS Test Statistic Computation

```

1: function KS2SAMPLE( $U, U^A, U^B$ )
   ▷ setup bin count leaf transformation circuit
2:    $pk_{\mathcal{L}_{BC}^s}, vk_{\mathcal{L}_{BC}^s} \leftarrow \text{Setup}(1^\lambda, \mathcal{L}_{BC}^s, \theta_{\mathcal{L}_{BC}^s})$ 
   ▷ setup bin count vector sum aggregation circuit
3:    $pk_{\mathcal{A}_{sum}^l}, vk_{\mathcal{A}_{sum}^l} \leftarrow \text{Setup}(1^\lambda, \mathcal{A}_{sum}^l, \theta_{\mathcal{A}_{sum}^l})$ 
   ▷ salted bin count CoSMETIC build on Group A
4:    $\Psi^A, H^{root,A} \leftarrow \text{COSMETICCROBUILD}(U, U^A, vk_{\mathcal{L}_{BC}^s}, vk_{\mathcal{A}_{sum}^l})$ 
   ▷ salted bin count CoSMETIC build on Group B
5:    $\Psi^B, H^{root,B} \leftarrow \text{COSMETICCROBUILD}(U, U^B, vk_{\mathcal{L}_{BC}^s}, vk_{\mathcal{A}_{sum}^l})$ 
   ▷ setup post-aggregation Max Absolute Gap circuit
6:    $pk_{MAG}, vk_{MAG} \leftarrow \text{Setup}(1^\lambda, \mathcal{G}_{MAG})$ 
7:   distribute  $vk_{MAG}$  to all users in  $U^A$  and  $U^B$ 
8:    $\zeta \leftarrow \text{MAXABSOLUTE GAP}(\Psi^A, \Psi^B)$ 
9:   set  $\Omega_{MAG} = \{\Psi^A, \Psi^B, \zeta\}$ 
10:  generate  $\Pi_{MAG} = \text{Prove}(pk_{MAG}, \Omega_{MAG})$ 
11:  distribute  $\Pi_{MAG}, pk_{MAG}$  publicly
12: end function

```

E.3 Logistic Likelihood-Ratio Test

We next evaluate the Logistic Likelihood-Ratio Test (LRT), which assesses the statistical significance of a full logistic regression model relative to a reduced baseline. The LRT computation process is

Algorithm 12 Verification Function for KS Test

```

1: function KSVERIFIER( $u, \text{vk}_{\mathcal{L}_{BC}^s}, \text{vk}_{\mathcal{A}_{sum}^l}$ )
2:    $\Phi^u \leftarrow \text{COSMETICVERIFIER}(u)$ 
3:    $\Phi^{MAG} \leftarrow \text{Verify}(\text{vk}_{MAG}, \Pi_{MAG},)$ 

  ▷ Verifications Conditions
4:   if  $\Phi^u$  and  $\Phi^{MAG}$  then
5:     if  $H^{root,A} = \text{hash}(\Psi^A)$  and  $H^{root,B} = \text{hash}(\Psi^B)$  then
6:       return verification successful
7:     else
8:       return Hashes not match.
9:     end if
10:   else
11:     return verification failed [ $\Phi^u, \Phi^{MAG}$ ]
12:   end if
13: end function

```

Algorithm 13 Maximum Absolute Gap Post-aggregation Function

```

1: function MAXABSOLUTEGAP( $\Psi^A, \Psi^B$ )
  ▷ compute CDF vectors
2:    $F_A = \text{CDF}(\Psi_A^K[0])$ 
3:    $F_B = \text{CDF}(\Psi_B^K[0])$ 

  ▷ compute maximum absolute gap
4:    $\zeta = \|F_A - F_B\|_\infty$  return  $\zeta$ 
5: end function

```

shown in Algorithm 14. The leaf-level transformation function is log-likelihood function, denoted by \mathcal{L}_{LL}^s , and the aggregation is performed using sum aggregator \mathcal{A}_{sum}^l . The parameters of the leaf transformation, $\theta_{\mathcal{L}_{LL}^s}$, correspond to the set of regression coefficients associated with a given logistic regression model. Within CoSMETIC, both full and reduced models are evaluated independently, and their log-likelihoods are combined through a zero-knowledge circuit to compute the LRT statistic (see Algorithm 15). The verification process for the LRT computation is described in Algorithm 16.

E.4 Logistic Accuracy (ACC) Test

Finally, we evaluate logistic regression accuracy (ACC), which measures classification performance under privacy-preserving computation (see Algorithm 17). We employ a classification assessment leaf transformation, denoted by \mathcal{L}_{CA}^s , which returns 1 if the predicted class matches the true class label and 0 otherwise. The parameters $\theta_{\mathcal{L}_{CA}^s}$ correspond to the logistic regression coefficients. The aggregation function, \mathcal{A}_{sum}^l , sums the assessed predictions across samples; this total is then divided by the sample size to obtain the overall classification accuracy.

Algorithm 14 Likelihood Ratio Test Computation

```

1: function LIKELIHOODRATIOTEST( $U, U^f, U^r$ )
  ▷ setup log likelihood leaf transformation circuit
2:    $\text{pk}_{\mathcal{L}_{LL}^s}, \text{vk}_{\mathcal{L}_{LL}^s} \leftarrow \text{Setup}(1^\lambda, \mathcal{L}_{LL}^s, \theta_{\mathcal{L}_{LL}^s})$ 

  ▷ setup log likelihood scalar sum aggregation circuit
3:    $\text{pk}_{\mathcal{A}_{sum}^l}, \text{vk}_{\mathcal{A}_{sum}^l} \leftarrow \text{Setup}(1^\lambda, \mathcal{A}_{sum}^l, \theta_{\mathcal{A}_{sum}^l})$ 

  ▷ salted log likelihood CoSMETIC build on full model
4:    $\Psi^f, H^{root,f} \leftarrow \text{COSMETICCROBUILD}(U, U^f, \text{vk}_{\mathcal{L}_{LL}^s}, \text{vk}_{\mathcal{A}_{sum}^l})$ 

  ▷ salted log likelihood CoSMETIC build on reduced model
5:    $\Psi^r, H^{root,r} \leftarrow \text{COSMETICCROBUILD}(U, U^r, \text{vk}_{\mathcal{L}_{LL}^s}, \text{vk}_{\mathcal{A}_{sum}^l})$ 

  ▷ setup post-aggregation LRT statistic circuit
6:    $\text{pk}_{LRT}, \text{vk}_{LRT} \leftarrow \text{Setup}(1^\lambda, \mathcal{G}_{LRT})$ 
7:   distribute  $\text{vk}_{LRT}$  to all users in  $U^f$  or  $U^r$ 
8:    $\zeta \leftarrow \text{LRTSTATISTIC}(\Psi^f, \Psi^r)$ 
9:   set  $\Omega_{LRT} = \{\Psi^f, \Psi^r, \zeta\}$ 
10:  generate  $\Pi_{LRT} = \text{Prove}(\text{pk}_{LRT}, \Omega_{LRT})$ 
11:  distribute  $\Pi_{LRT}, \text{pk}_{LRT}$  publicly
12: end function

```

Algorithm 15 LRT Statistic Post Aggregation Function

```

1: function LRTSTATISTIC( $\Psi^f, \Psi^r$ )
  ▷ LRT Statistic
2:    $\zeta = -2 \times (\Psi^r - \Psi^f)$ 
3:   return  $\zeta$ 
4: end function

```

Algorithm 16 Verification Function for LRT Test

```

1: function LRTVERIFIER( $u, \text{vk}_{\mathcal{L}_{LL}^s}, \text{vk}_{\mathcal{A}_{sum}^l}$ )
2:    $\Phi^u \leftarrow \text{COSMETICVERIFIER}(u)$ 
3:    $\Phi^{LL} \leftarrow \text{Verify}(\text{vk}_{LL}, \Pi_{LL})$ 
  ▷ Verifications Conditions
4:   if  $\Phi^u$  and  $\Phi^{LL}$  then
5:     if  $H^{root,f} = \text{hash}(\Psi^f)$  and  $H^{root,r} = \text{hash}(\Psi^r)$  then
6:       return verification successful
7:     else
8:       return Hashes not match.
9:     end if
10:   else
11:     return verification failed [ $\Phi^u, \Phi^{LL}$ ]
12:   end if
13: end function

```

F Supplementary Results**F.1** Cryptographic Overhead and Key Size

We present the key sizes for proving and verification keys across KS, LR and Acc tests as presented in Tables Table 6, Table 7 and Table 8. The associated cryptographic costs of the KS test are shown in Table 6. Proving keys for both KS transformers remain stable at approximately 11.3 GB, while verification keys remain below 3 MB.

Algorithm 17 Accuracy Computation

```

1: function ACCURACY( $U, U^{test}$ )
   ▷ setup classification assessment leaf transformation circuit
2:  $pk_{\mathcal{L}_{CA}^s}, vk_{\mathcal{L}_{CA}^s} \leftarrow \text{Setup}(1^\lambda, \mathcal{L}_{CA}^s, \theta_{\mathcal{L}_{CA}^s})$ 
   ▷ setup classification assessment sum aggregation circuit
3:  $pk_{\mathcal{A}_{sum}^l}, vk_{\mathcal{A}_{sum}^l} \leftarrow \text{Setup}(1^\lambda, \mathcal{A}_{sum}^l, \theta_{\mathcal{A}_{sum}^l})$ 
   ▷ salted classification assessment CoSMeTIC on test sample
4:  $\Psi, H^{root} \leftarrow \text{COSMETICCROBUILD}(U, U^{test}, vk_{\mathcal{L}_{CA}^s}, vk_{\mathcal{A}_{sum}^l})$ 
5:  $pk_{ACC}, vk_{ACC} \leftarrow \text{Setup}(1^\lambda, \mathcal{G}_{ACC})$ 
6: distribute  $vk_{ACC}$  to all users in  $U^{test}$ 
7: set  $\Omega_{ACC} = \{\Psi\}$ 
8: generate  $\Pi_{ACC} = \text{Prove}(pk_{ACC}, \Omega_{ACC})$ 
9: distribute  $\Pi_{ACC}, pk_{ACC}$  publicly
10: end function

```

Algorithm 18 Verification Function for ACC

```

1: function LRTVERIFIER( $u, vk_{\mathcal{L}_{CA}^s}, vk_{\mathcal{A}_{sum}^l}$ )
2:  $\Phi^u \leftarrow \text{COSMETICVERIFIER}(u)$ 
3:  $\Phi^{CA} \leftarrow \text{Verify}(vk_{CA}, \Pi_{CA}, )$ 
4: if  $\Phi^u$  and  $\Phi^{CA}$  then
5:   return verification successful
6: else
7:   return verification failed [ $\Phi^u, \Phi^{CA}$ ]
8: end if
9: end function

```

EZKL Scale	Model 1				Model 2			
	LTR		MRP		LTR		MRP	
	PK	VK	PK	VK	PK	VK	PK	VK
8	11.27	2.69	10.29	2.43	11.27	2.69	10.29	2.43
10	11.27	2.69	10.29	2.43	11.27	2.69	10.29	2.43
12	11.27	2.69	10.29	2.43	11.27	2.69	10.29	2.43
14	11.27	2.69	10.29	2.43	11.27	2.69	10.29	2.43

Table 6: KS Proving(GB) and verification(MB) key sizes across EZKL Scale

EZKL Scale	Full				Reduced			
	LTR		MRP		LTR		MRP	
	PK	VK	PK	VK	PK	VK	PK	VK
8	11.27	2.69	10.29	2.43	11.27	2.69	10.29	2.43
10	11.27	2.69	10.29	2.43	11.27	2.69	10.29	2.43
12	11.27	2.69	10.29	2.43	11.27	2.69	10.29	2.43
14	11.27	2.69	10.29	2.43	11.27	2.69	10.29	2.43

Table 7: LRT Proving(GB) and verification(MB) key sizes across EZKL Scale

The Max Gap transformer incurs a modest increase in proving key size due to its comparative logic; however, this overhead remains constant across precision scales. These results show that KS-based distribution testing can be embedded into cryptographic statistical models without introducing scale-dependent cryptographic growth.

The corresponding cryptographic overhead for the LR test is reported in Table 7. Proving keys for both the full and reduced models remain near 11.3 GB, while verification keys stay close

EZKL Scale	Length				Acc			
	LTR		MRP		LTR		MRP	
	PK	VK	PK	VK	PK	VK	PK	VK
8	11.27	2.69	10.29	2.43	13.24	3.07	10.29	2.43
10	11.27	2.69	10.29	2.43	13.24	3.07	10.29	2.43
12	11.27	2.69	10.29	2.43	13.24	3.07	10.29	2.43
14	11.27	2.69	10.29	2.43	13.24	3.07	10.29	2.43

Table 8: ACC Proving(GB) and verification(MB) key sizes across EZKL Scale

to 2.7 MB. The LRT statistic transformer does not introduce unexpected overhead, and the associated MRP components remain unchanged across precision settings. These results indicate that CoSMeTIC supports complex regression-based inference without amplifying cryptographic costs. The corresponding cryptographic costs for the ACC test are shown in Table 8. Proving keys remain stable across scales for both transformers, and verification keys remain within a narrow megabyte range.